Relativistic description of inclusive quasielastic proton-nucleus scattering with relativistic distorted-wave impulse approximation and random-phase approximation

D. D. van Niekerk,* B. I. S. van der Ventel,† and N. P. Titus‡
Department of Physics, Stellenbosch University, Private Bag X1, Matieland 7602, South Africa

G. C. Hillhouse
University for Information Science and Technology, Building at ARM, Partizanska Street, Ohrid 6000, Republic of Macedonia
(Received 22 November 2010; revised manuscript received 18 January 2011; published 13 April 2011)

We present a fully relativistic model for polarized inclusive quasielastic proton-nucleus scattering that includes relativistic distorted waves for the projectile and ejectile (RDWIA), as well as the relativistic random-phase approximation (RPA) applied to the target nucleus. Using a standard relativistic impulse approximation treatment of quasielastic scattering and a two-body Scalar, Pseudoscalar, Vector, Axial vector, Tensor (SPVAT) form of the current operator, it is shown how the behavior of the projectile/ejectile and target can be decoupled. Distortion effects are included via a full partial-wave expansion of the relativistic wave functions. Target correlations are included via the relativistic RPA applied to mean-field theory in quantum hadrodynamics. A number of novel analytical and numerical techniques are employed to aid in this highly nontrivial calculation. A baseline plane-wave calculation is performed for the reaction ^{40}Ca$(\vec{p}, \vec{p}\,')$ at an energy of 500 MeV and an angle $\theta_{\text{c.m.}} = 40^\circ$. Here it is found that the effect of isoscalar correlations is a quenching of the cross section that is expected to become more pronounced at lower energies or for higher-density targets. A RDWIA calculation shows additional reduction and if isoscalar target correlations are included this effect is enhanced.

DOI: 10.1103/PhysRevC.83.044607 PACS number(s): 24.10.Jv, 24.70.+s, 25.40.−h

I. INTRODUCTION

With newly commissioned radioactive beam facilities such as RIKEN in Japan, GSI Facility for Antiproton and Ion Research in Germany, and Facility for Rare Isotope Beams in the United States, where the goal is to extend the nuclear landscape to the drip lines, many changes are expected to be observed in the structure of exotic nuclei. However, understanding these is tied to our understanding of the reactions that will be used to probe them, such as elastic and inelastic proton-nucleus scattering.

In contrast to elastic collisions which are only sensitive to scalar and vector (isoscalar) pieces of the nucleon-nucleon (NN) scattering amplitudes, inelastic reactions are sensitive to all [1]. When results are compared to those of free NN scattering, inelastic scattering spin observables and cross sections can shed new light on nuclear structure because changes in scattering observables are likely attributable to changes in the collective response of the target or from a medium-modification of the free NN interaction [2]. Among these, quasifree (or quasielastic) scattering, a single-step surface peaked reaction whereby a projectile interacts with a single bound nucleon in the target nucleus, is considered to be the dominant mechanism for nuclear excitation at moderate momentum transfers ($1 \leqslant q \leqslant 2$ fm^{-1}) and energies between 100 and 500 MeV [3]. Details of nuclear structure and excited states are unimportant for quasielastic scattering and compared to elastic scattering it offers a wider range of spin observables [4,5].

Quasielastic scattering manifests itself in the cross section as a peak close to the excitation energy of free NN scattering with a width ascribable to the Fermi motion of the target nucleons. The centroid of the quasielastic peak also moves according to NN energy and momentum conservation and the peak position ($\omega = \mathbf{q}^2/2M$) and width ($\Delta\omega = |\mathbf{q}|k_F/M$) do not vary significantly with target mass, confirming that the reaction mechanism is dominated by a single-step process [3,6]. Multiple scattering events are expected to be less than 10% at the quasielastic peak. On the high-energy-loss side, however, between the peak and the appearance of resonances (owing to meson production), this effect can play an important role affecting the strength observed in the cross section, as well as the the spin observables [1,6,7].

It has been established that inclusive spectra for targets with mass numbers less than 60 and laboratory scattering angles less than 25° exhibit clear quasielastic peaks that become more pronounced with increasing beam energy and broadens and drops with an increase in the angle [8,9].

The model presented here has been formulated to describe inclusive quasielastic proton-nucleus scattering. The quasielastic nature of the process leads to the assumption that the many-body interaction can be modeled by a two-body current operator in the impulse approximation. We make use of the IA1 Scalar, Pseudoscalar, Vector, Axial vector, Tensor (SPVAT) representation of the NN amplitudes as presented in Ref. [10]. Despite not incorporating Pauli blocking and binding energy corrections, this parametrization is expected to be adequate for the relatively low density of the nuclear surface where quasielastic scattering is assumed to be localized [11]. This form of the amplitudes has been successfully employed in impulse approximation descriptions of both elastic [12,13] and quasielastic scattering [1,4].

*ddvniekerk@sun.ac.za
†bventel@sun.ac.za
‡nortin@sun.ac.za

An important feature of the model is the separation of the projectile/ejectile and target behaviors into two separate and independent, so-called hadronic and polarization tensors. Subsequently, either plane waves (RPWIA) or distorted waves (RDWIA) can be used to determine the hadronic tensor.

In contrast to the RPWIA model of Horowitz and Murdock [1,4], where relativistic effects are included via the effective nucleon masses, RDWIA incorporates these effects by generating the projectile and ejectile wave functions as solutions of the Dirac equation with relativistic potentials.

Overall the RPWIA has had mixed success in describing complete sets of spin observables [3,14]. In Ref. [1] a fully relativistic distorted wave (RDWIA) calculation is recommended to gauge the effect of distortions on the spin-orbit interaction. In Ref. [15] it was found that the magnitude of the analyzing power for ^{54}Fe($\vec{p}$, $\vec{p}\,'$) is accurately reproduced but the slope as a function of energy is not. In the context of nonrelativistic models it has also been shown that whereas the PWIA reproduces fairly well the position and width of the quasielastic peak, DWIA provides the correct normalization [6]. Because spin observables are, in effect, ratios of polarized double differential cross sections they are, however, not expected to be significantly modified by distortions [11]. Nevertheless, as the incident energy is lowered and the target mass increased the effect of distortions is expected to become more pronounced [3]. Nonrelativistic calculations suggest that distortion effects can noticeably affect the shape and position of the quasielastic peak [16,17]. Although hard scattering may occur at the center of the quasielastic peak, distortions may play a role off the peak affecting spin observables and changing the slope of a spin observable with respect to excitation energy [1] and fully relativistic DWIA calculations could be used to investigate this.

In our model the lowest-order relativistic response of the nucleus is provided by the relativistic mean-field or Hartree approximation of the Walecka ($\sigma\omega$) model [18].

The nucleus is modeled as a Fermi gas of nucleons where the interaction is mediated by the exchange of scalar and vector isoscalar mesons. This interaction is modeled in nuclear matter which leads to constant potentials that only affect the mass of the nucleons. It has been shown that many phenomena in nuclear matter and finite nuclei can be explained as a relativistic effect in this framework [18–22].

Specifically, the response of the target is calculated in mean-field theory (MFT) where vacuum effects are neglected. We make use of the Walecka model (QHD-I) where ground-state (bulk) properties are determined by isoscalar mesons [20]. Parameters of the MFT model (masses of mesons and coupling constants) are determined from the ground-state properties of ^{40}Ca [19,23]. Even though the relativistic Hartree approximation (RHA), which includes vacuum effects, may be conceptually more complete, the role of vacuum polarization in effective hadronic field theories is currently being revisited [20,21,24,25]. Serot and Walecka [22] feel that inclusion of vacuum effects is essential to maintain the completeness of the Dirac basis, which plays a crucial role in field theory, but that the current description of the vacuum by summing simple baryon loops is inadequate. Horowitz and Piekarewicz [26] have also suggested that some of the differences between MFT and RHA calculations may not be attributable to the inclusion of vacuum effects but rather the different effective masses and meson couplings.

The interaction of a nucleon with the many-body medium of the nucleus can excite particle-hole and particle-antiparticle pairs and in a dense system these excitations can propagate via the interactions of the constituents [27]. In the context of MFT the random-phase approximation (RPA) improves on the simple single-particle response by including the effects of long-range coherence among particle-hole excitations by iterating lowest-order (uncorrelated) polarizations to infinite order [28,29]. We therefore investigate the effects of residual isoscalar particle-hole correlations by means of RPA. Reference [20] notes that a consistent treatment of excited states in the Hartree approximation constrains only isoscalar particle-hole correlations significantly. Isovector RPA (as discussed in Ref. [2]) applied to the present model is a subject of future work.

The relativistic RPA has been quite successful in the calculation of electromagnetic responses of nuclei [30–36], where it has consistently been shown to be in better agreement with experimental data than the lowest-order (Hartree) response (both in nuclear matter and finite nucleus calculations). In general it has been noted that RPA correlations shift strength downward owing to the attractive particle-hole interactions [26].

Reference [2] examines spin observables for quasielastic ($\vec{p}$, $\vec{n}$) scattering in the RPWIA. Nuclear response functions are calculated in an isovector RPA to the Walecka model. They find better agreement with data for all spin observables calculated in RRPA when compared to the Hartree approximation as well as Fermi gas (free mass) RPA. A calculation that includes both distortions as well as RRPA is suggested for further improvement of theoretical predictions.

The paper is organized as follows: In Sec. II we present the formalism and discuss the different assumptions and approximations. Section III discusses some calculational procedures and computational techniques and subsequently Sec. IV presents the polarized double differential cross section calculations with and without RPA corrections for both the RPWIA and the RDWIA. Section V contains a summary of our results, conclusions, and recommendations for future work.

II. FORMALISM

A. Cross section

As shown in Ref. [37] we start by considering the differential cross section of a proton and nucleus shown in Fig. 1. This is given by [38]

$$d\sigma = \frac{1}{|\mathbf{v}_1 - \mathbf{v}_2|}\left(\frac{M^2}{E(\mathbf{k})E(\mathbf{k}')}\right)(2\pi)^4\delta(k + K - k' - K') \times \frac{d^3k'}{(2\pi)^3}\frac{d^3K'}{(2\pi)^3}|\mathcal{M}|^2, \quad (1)$$

where $\mathbf{v}_1$ and $\mathbf{v}_2$ are the velocities of the projectile and target nucleus, respectively, k and k' are the asymptotic four-momenta of the projectile and ejectile nucleons, K and K' are the asymptotic four-momenta of the target and residual nucleus, M is the free nucleon mass, and $\mathcal{M}$ is the transition matrix element.

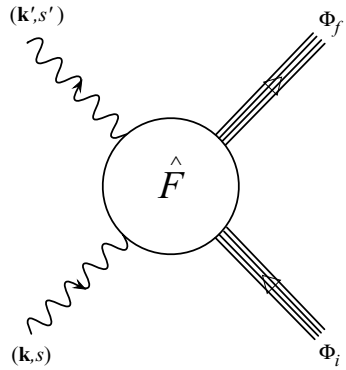

FIG. 1. Diagrammatic representation of quasielastic nucleon-nucleus scattering. $(\mathbf{k}, s)\,[(\mathbf{k}', s')]$ represents the asymptotic momenta and spin projection of the initial [final] nucleon, Φ_i (Φ_f) the initial (final) states of the nucleus and $\hat{F}$ the NN interaction matrix.

Because we are interested in inclusive scattering, we sum over final nuclear states and in the center-of-mass frame the polarized double differential cross section is therefore given by

$$\frac{d\sigma}{dE'\,d\Omega'} = -\frac{1}{\pi}\mathcal{K}\mathrm{Im}\left\{\sum_n |\mathcal{M}|^2 \frac{1}{\omega - (E_n - E_0) + i\epsilon}\right\}, \tag{2}$$

with $\mathcal{K}$ a kinematic factor:

$$\mathcal{K} = \frac{M^2|\mathbf{k}'|\left(\mathbf{k}^2 + M^2_{\text{target}}\right)^{\frac{1}{2}}}{4\pi^2|\mathbf{k}|\left[(\mathbf{k}^2 + M^2)^{\frac{1}{2}} + \left(\mathbf{k}^2 + M^2_{\text{target}}\right)^{\frac{1}{2}}\right]}. \tag{3}$$

As it stands, the transition matrix element is a fundamental many-body quantity describing the transition of an initial many-body state to a final many-body state via the action of the many-body operator $\hat{F}_{\text{many}}$:

$$\begin{aligned}\mathcal{M} = \int d^4x\, d^4x' \prod_{m=1}^{A} d^4y_m \prod_{n=1}^{A} d^4y'_n \\ \times [\bar{\psi}^{(-)}(x', \mathbf{k}', \hat{i}', s') \otimes \bar{\Phi}_f(y'_1, \ldots, y'_n, \ldots, y'_A)] \\ \times \hat{F}_{\text{many}}(x, x', \{y\}, \{y'\}) \\ \times [\psi^{(+)}(x, \mathbf{k}, \hat{i}, s) \otimes \Phi_i(y_1, \ldots, y_m, \ldots, y_A)],\end{aligned} \tag{4}$$

where

(i) $\otimes$ denotes the Kronecker product;
(ii) $\psi^{(+)}(x, \mathbf{k}, \hat{i}, s)$ is the relativistic distorted wave function of the projectile with outgoing boundary conditions [indicated by superscript $(+)$], asymptotic three-momentum $\mathbf{k}$ in the proton-nucleus center-of-mass system, spin projection s along an arbitrary quantization axis $\hat{i}$ in the rest frame of the projectile (see Appendix D);
(iii) $\psi^{(-)}(x', \mathbf{k}', \hat{i}', s')$ is the relativistic distorted wave function of the ejectile with incoming boundary conditions [indicated by superscript $(-)$], asymptotic three-momentum $\mathbf{k}'$ in the proton-nucleus center-of-mass system, spin projection s' along an arbitrary quantization axis $\hat{i}'$ in the rest frame of the ejectile (see Appendix D);
(iv) $\Phi_i(y_1, \ldots, y_i, \ldots, y_A)$ is the many-body ground state of the target nucleus, which depends on all A constituent nucleons;
(v) $\Phi_f(y'_1, \ldots, y'_j, \ldots, y'_A)$ is the many-body ground state of the recoil nucleus, which depends on all A constituent nucleons;
(vi) $\hat{F}_{\text{many}}$ is the many-body operator that connects the initial and final states.

Because we model the scattering as a quasielastic process where the interaction takes place between the projectile and a single nucleon inside the target nucleus, we approximate the many-body operator as

$$\hat{F}_{\text{many}}(x, x', \{y\}, \{y'\}) = \sum_{i=1}^{A} \langle x' y'_i | \hat{F} | x y_i \rangle \prod_{j=1, i\neq j}^{A} \delta(y'_j - y_j), \tag{5}$$

where $\hat{F}$ is a two-body operator. With the form of the many-body operator given in Eq. (5) the transition matrix element becomes

$$\begin{aligned}\mathcal{M} = \sum_{i=1}^{A} \int d^4x\, d^4x'\, d^4y_i\, d^4y'_i \prod_{j=1, i\neq j}^{A} d^4y_j \\ \times [\bar{\psi}^{(-)}(x', \mathbf{k}', \hat{i}', s') \otimes \bar{\Phi}_f(y_1, \ldots, y'_i, \ldots, y_A)] \\ \times \langle x' y'_i | \hat{F} | x y_i \rangle \\ \times [\psi^{(+)}(x, \mathbf{k}, \hat{i}, s) \otimes \Phi_i(y_1, \ldots, y_i, \ldots, y_A)],\end{aligned} \tag{6}$$

where use was made of the fact that

$$\begin{aligned}\int \sum_{i}^{A} \prod_{m}^{A} d^4y_m \prod_{n}^{A} d^4y'_n \prod_{j\neq i}^{A} \delta(y'_j - y_j) \\ \equiv \int \sum_{i}^{A} d^4y_i\, d^4y'_i \prod_{j\neq i}^{A} d^4y_j.\end{aligned} \tag{7}$$

If we insert complete sets of eigenstates defined by

$$1 = \int \frac{d^4p}{(2\pi)^4} |p\rangle\langle p|, \tag{8}$$

we obtain

$$\begin{aligned}\mathcal{M} = \sum_{i=1}^{A} \int d^4x\, d^4x'\, d^4y_i\, d^4y'_i \prod_{j=1, j\neq i}^{A} d^4y_j \frac{d^4p}{(2\pi)^4}\frac{d^4p'}{(2\pi)^4} \\ \times \frac{d^4p_i}{(2\pi)^4}\frac{d^4p'_i}{(2\pi)^4} e^{ip\cdot x} e^{-ip'\cdot x'} e^{ip_i\cdot y_i} e^{-ip'_i\cdot y'_i} \\ \times [\bar{\psi}^{(-)}(x', \mathbf{k}', \hat{i}', s') \otimes \bar{\Phi}_f(y_1, \ldots, y'_i, \ldots, y_A)] \\ \times \langle p' p'_i | \hat{F} | p\, p_i \rangle \\ \times [\psi^{(+)}(x, \mathbf{k}, \hat{i}, s) \otimes \Phi_i(y_1, \ldots, y_i, \ldots, y_A)],\end{aligned} \tag{9}$$

where we have used

$$\langle x | p \rangle = e^{-ip\cdot x}. \tag{10}$$

If we assume that the time dependence of the wave functions is given by

$$\psi^{(+)}(x, \mathbf{k}, \hat{i}, s) = e^{-iE(\mathbf{k})x_0}\psi^{(+)}(\mathbf{x}, \mathbf{k}, \hat{i}, s), \quad (11)$$

$$\bar{\psi}^{(-)}(x', \mathbf{k}', \hat{i}', s') = e^{iE(\mathbf{k}')x'_0}\bar{\psi}^{(-)}(\mathbf{x}', \mathbf{k}', \hat{i}', s'), \quad (12)$$

$$\Phi_i(y_1, \ldots, y_i, \ldots, y_A) = \left[\prod_{m=1, m\neq i}^{A} e^{-iK_{m,0}y_{m,0}}\right] e^{-iK_{i,0}y_{i,0}} \times \Phi_i(\mathbf{y}_1, \ldots, \mathbf{y}_i, \ldots, \mathbf{y}_A), \quad (13)$$

$$\bar{\Phi}_f(y_1, \ldots, y'_i, \ldots, y_A) = \left[\prod_{n=1, n\neq i}^{A} e^{iK'_{n,0}y_{n,0}}\right] e^{iK'_{i,0}y'_{i,0}} \times \bar{\Phi}_f(\mathbf{y}_1, \ldots, \mathbf{y}'_i, \ldots, \mathbf{y}_A), \quad (14)$$

we can perform the integration over the timelike components of the spatial four-vectors using the identity

$$\int dx_0\, e^{ix[p_0 - E(\mathbf{k})]} = 2\pi\, \delta[p_0 - E(\mathbf{k})] \quad (15)$$

for every coordinate to obtain $\delta[p_0 - E(\mathbf{k})]\,\delta[p'_0 - E(\mathbf{k}')]\delta(p_{i,0} - K_{i,0})\delta(p'_{i,0} - K'_{i,0})$. These δ functions can be used to perform the integrals over p_0, p'_0, $p_{i,0}$ and $p'_{i,0}$ (which fixes these components), resulting in

$$\begin{aligned}\mathcal{M} = \sum_{i=1}^{A} \Delta_i \int d^3x\, d^3x'\, d^3y_i\, d^3y'_i \prod_{j=1, j\neq i}^{A} d^3y_j \frac{d^3p}{(2\pi)^3}\frac{d^3p'}{(2\pi)^3} \\ \times \frac{d^3p_i}{(2\pi)^3}\frac{d^3p'_i}{(2\pi)^3} e^{-i\mathbf{p}\cdot\mathbf{x}} e^{i\mathbf{p}'\cdot\mathbf{x}'} e^{-i\mathbf{p}_i\cdot\mathbf{y}_i} e^{i\mathbf{p}'_i\cdot\mathbf{y}'_i} \\ \times [\bar{\psi}^{(-)}(\mathbf{x}', \mathbf{k}', \hat{i}', s') \otimes \bar{\Phi}_f(\mathbf{y}_1, \ldots \mathbf{y}'_i, \ldots \mathbf{y}_A)] \\ \times \langle p' p'_i | \hat{F} | p\ p_i\rangle \\ \times [\psi^{(+)}(\mathbf{x}, \mathbf{k}, \hat{i}, s) \otimes \Phi_i(\mathbf{y}_1, \ldots \mathbf{y}_i, \ldots \mathbf{y}_A)], \end{aligned} \quad (16)$$

with

$$\begin{aligned}\Delta_i &= \int \prod_{j=1, j\neq i}^{A} dy_{j,0} \left\{ \prod_{m=1, m\neq i}^{A} e^{-iK_{m,0}y_{m,0}} \prod_{n=1, n\neq i}^{A} e^{iK'_{n,0}y_{n,0}} \right\} \\ &= \int \prod_{j=1, j\neq i}^{A} dy_{j,0}\, e^{-iK_{j,0}y_{j,0}} e^{iK'_{j,0}y_{j,0}} \\ &= \prod_{j=1, j\neq i}^{A} \delta(K'_{j,0} - K_{j,0}). \end{aligned} \quad (17)$$

The energies of the spectator nucleons present here in the product of δ functions can be integrated out.

To proceed, a specific representation for the operator $\hat{F}$ has to be chosen. We use

$$\langle p' p'_i | \hat{F} | p\ p_i\rangle = (2\pi)^3 \delta(\mathbf{p} + \mathbf{p}_i - \mathbf{p}' - \mathbf{p}'_i) \times \sum_{L=S}^{T} F_L(p, p_i, p', p'_i)(\lambda^L \otimes \lambda_L). \quad (18)$$

This is the well-known SPVAT form which has been successfully employed in elastic [39–41], quasielastic [1,42], and inelastic proton-nucleus scattering [43,44], where $\lambda^L \in \{I_4, \gamma^5, \gamma^\mu, \gamma^5\gamma^\mu, \sigma^{\mu\nu}\}$; that is, $L = S, P, V, A, T$, and F_L is the complex NN amplitude. Note that three-momentum conservation is explicitly enforced. In the expression for λ^L we adopt the conventions of Ref. [38]. Substituting the representation for the operator $\hat{F}$ shown in Eq. (18) into Eq. (16) and subsequent integration over $\mathbf{p}'_i$ results in

$$\begin{aligned}\mathcal{M} = \sum_{i=1}^{A}\sum_{L=S}^{T} \int d^3x\, d^3x'\, d^3y_i\, d^3y'_i \prod_{j=1, j\neq i}^{A} d^3y_j \frac{d^3p}{(2\pi)^3}\frac{d^3p'}{(2\pi)^3} \\ \times \frac{d^3p_i}{(2\pi)^3} e^{i\mathbf{p}\cdot(\mathbf{y}'_i - \mathbf{x})} e^{i\mathbf{p}'\cdot(\mathbf{x}' - \mathbf{y}'_i)} e^{i\mathbf{p}_i\cdot(\mathbf{y}'_i - \mathbf{y}_i)} F_L(p, p_i, p', p'_i) \\ \times [\bar{\psi}^{(-)}(\mathbf{x}', \mathbf{k}', \hat{i}', s')\lambda^L \psi^{(+)}(\mathbf{x}, \mathbf{k}, \hat{i}, s)] \\ \times [\bar{\Phi}_f(\mathbf{y}_1, \ldots, \mathbf{y}'_i, \ldots, \mathbf{y}_A)\lambda_L \Phi_i(\mathbf{y}_1, \ldots, \mathbf{y}_i, \ldots, \mathbf{y}_A)]. \end{aligned} \quad (19)$$

Note that although the amplitude appears to depend on the momentum four-vectors in Eq. (19), the zeroth components are fixed [see Eq. (15)]. In addition, we invoke the impulse approximation whereby the interaction between two nucleons in the nuclear medium is assumed to be identical to the free-space interaction. The NN interaction is thus fully determined by on-shell two-nucleon data [1,43,45]. This amounts to a relativistic parametrization of the Arndt phases [1]. We therefore make the approximation that the NN amplitudes are evaluated at a fixed value of the asymptotic momentum $\mathbf{K}_i$ of the target nucleon in the center-of-mass frame [3,43,46] and we make the replacement

$$F_L(p, p_i, p', p'_i) \to F_L(\mathbf{k}, \mathbf{K}_i, \mathbf{k}') \equiv F_L(T_{\rm lab}, |\mathbf{q}|), \quad (20)$$

where $\mathbf{q} = \mathbf{k} - \mathbf{k}'$. Note that this method of calculating the amplitudes does not address the off-shell problem and the latter should be the subject of further study in relativistic models of nuclear scattering processes.

The remaining integrals over the momenta $\mathbf{p}$, $\mathbf{p}'$, and $\mathbf{p}_i$ can be performed and results in the δ functions $\delta(\mathbf{y}'_i - \mathbf{x})$ $\delta(\mathbf{x}' - \mathbf{y}'_i)\delta(\mathbf{y}'_i - \mathbf{y}_i)$. Performing the integral over $\mathbf{y}'_i$ results in

$$\begin{aligned}\mathcal{M} = \sum_{i=1}^{A}\sum_{L=S}^{T} \int d^3x\, d^3x'\, d^3y_i \prod_{j=1, j\neq i}^{A} d^3y_j\, F_L(T_{\rm lab}, |\mathbf{q}|) \\ \times [\bar{\psi}^{(-)}(\mathbf{x}', \mathbf{k}', \hat{i}', s')\lambda^L \psi^{(+)}(\mathbf{x}, \mathbf{k}, \hat{i}, s)] \\ \times [\bar{\Phi}_f(\mathbf{y}_1, \ldots, \mathbf{y}_i, \ldots, \mathbf{y}_A)\lambda_L \Phi_i(\mathbf{y}_1, \ldots, \mathbf{y}_i, \ldots, \mathbf{y}_A)] \\ \times \delta(\mathbf{y}_i - \mathbf{x})\delta(\mathbf{x}' - \mathbf{y}_i). \end{aligned} \quad (21)$$

Consistent with the basic assumption of quasielastic scattering, we assume that the many-body operator, λ_L, has a simple one-body form. We define the initial and final nuclear states in terms of Slater determinants as

$$\Phi_i = \frac{1}{\sqrt{A!}} \det\left[\phi_n^{(i)}(\mathbf{y}_k)\right]_{n=1,\ldots,A,\, k=1,\ldots,A}, \quad (22)$$

$$\Phi_f = \frac{1}{\sqrt{A!}} \det\left[\phi_m^{(f)}(\mathbf{y}_k)\right]_{m=1,\ldots,A,\, k=1,\ldots,A}. \quad (23)$$

Because the initial and final nuclear states differ only by a single one-particle state, the action of the operator λ_L, which sees only the ith particle, can be written as

$$\int \prod_{j=1, j\neq i}^{A} d^3y_j\, \bar{\Phi}_f \lambda_L^{(i)} \Phi_i = \frac{1}{A}\langle \Phi_f | \hat{\bar{\phi}}(\mathbf{y}_i)\lambda_L \hat{\phi}(\mathbf{y}_i) | \Phi_i\rangle, \quad (24)$$

where $\hat{\phi}$ is the Heisenberg field operator. Substitution of this expression into Eq. (21) and subsequent integration over $\mathbf{y}_i$ and $\mathbf{x}'$ results in

$$\begin{aligned}\mathcal{M} &= \sum_{i=1}^{A}\frac{1}{A}\sum_{L=S}^{T}\int d^3x\, F_L(T_{\rm lab},|\mathbf{q}|)\\ &\quad\times[\bar{\psi}^{(-)}(\mathbf{x},\mathbf{k}',\hat{\imath}',s')\lambda^L\psi^{(+)}(\mathbf{x},\mathbf{k},\hat{\imath},s)]\\ &\quad\times\langle\Phi_f|\hat{\bar{\phi}}(\mathbf{x})\lambda_L\hat{\phi}(\mathbf{x})|\Phi_i\rangle\\ &= \sum_{L=S}^{T}\int d^3x\, F_L(T_{\rm lab},|\mathbf{q}|)\\ &\quad\times[\bar{\psi}^{(-)}(\mathbf{x},\mathbf{k}',\hat{\imath}',s')\lambda^L\psi^{(+)}(\mathbf{x},\mathbf{k},\hat{\imath},s)]\\ &\quad\times\langle\Phi_f|\hat{\bar{\phi}}(\mathbf{x})\lambda_L\hat{\phi}(\mathbf{x})|\Phi_i\rangle,\end{aligned}\tag{25}$$

from which it follows that

$$\begin{aligned}\frac{d\sigma}{dE'\,d\Omega'} &= -\frac{1}{\pi}\mathcal{K}\,\mathrm{Im}\left\{\sum_{L,L'=S}^{T}F_L(T_{\rm lab},|\mathbf{q}|)F^*_{L'}(T_{\rm lab},|\mathbf{q}|)\right.\\ &\quad\left.\times\int d^3x\,d^3y\,H^{LL'}(\mathbf{x},\mathbf{y})\Pi_{LL'}(\mathbf{x},\mathbf{y},\omega)\right\},\end{aligned}\tag{26}$$

where we have defined the hadronic tensor $H^{LL'}(\mathbf{x},\mathbf{y})$,

$$\begin{aligned}H^{LL'}(\mathbf{x},\mathbf{y}) &= [\bar{\psi}^{(-)}(\mathbf{x},\mathbf{k}',\hat{\imath}',s')\lambda^L\psi^{(+)}(\mathbf{x},\mathbf{k},\hat{\imath},s)]\\ &\quad\times[\bar{\psi}^{(+)}(\mathbf{y},\mathbf{k},\hat{\imath},s)\overline{\lambda_{L'}}\psi^{(-)}(\mathbf{y},\mathbf{k}',\hat{\imath}',s')],\end{aligned}\tag{27}$$

and the polarization tensor $\Pi_{LL'}(\mathbf{x},\mathbf{y},\omega)$,

$$\begin{aligned}\Pi_{LL'}(\mathbf{x},\mathbf{y},\omega) &= \sum_n\left[\frac{\langle n|\hat{\bar{\phi}}(\mathbf{x})\lambda_L\hat{\phi}(\mathbf{x})|0\rangle\langle 0|\hat{\bar{\phi}}(\mathbf{y})\overline{\lambda_{L'}}\hat{\phi}(\mathbf{y})|n\rangle}{\omega-(E_n-E_0)+i\epsilon}\right.\\ &\quad\left.+\frac{\langle n|\hat{\bar{\phi}}(\mathbf{y})\overline{\lambda_{L'}}\hat{\phi}(\mathbf{y})|0\rangle\langle 0|\hat{\bar{\phi}}(\mathbf{x})\lambda_L\hat{\phi}(\mathbf{x})|n\rangle}{\omega+(E_n-E_0)-i\epsilon}\right].\end{aligned}\tag{28}$$

In Eq. (28) the second term has been added to write the result in terms of a time-ordered product [21]. This can be done because the energy transferred to the nucleus is always positive and the contribution of this term to the cross section is therefore zero. Note that $|0\rangle$ is the initial interacting many-body ground state (initial state of the nucleus) and $|n\rangle$ similarly the final state. Both are eigenstates of the full Hamilton operator. Because we consider only single-particle field operators, we take into account only one-particle-one-hole excitations. Note also that

$$\overline{\lambda_{L'}} = \gamma^0\lambda^\dagger_{L'}\gamma^0.$$

In the nuclear-matter approximation the polarization tensor can be written as

$$\Pi_{LL'}(\mathbf{x},\mathbf{y},\omega) = \int\frac{d^3q}{(2\pi)^3}e^{-i\mathbf{q}\cdot(\mathbf{x}-\mathbf{y})}\Pi_{LL'}(\mathbf{q},\omega),\tag{29}$$

which results in

$$\begin{aligned}\frac{d\sigma}{dE'\,d\Omega'} &= -\frac{1}{\pi}\mathcal{K}\,\mathrm{Im}\left\{\sum_{L,L'=S}^{T}F_L(T_{\rm lab},|\mathbf{q}|)F^*_{L'}(T_{\rm lab},|\mathbf{q}|)\right.\\ &\quad\left.\times\int\frac{d^3q}{(2\pi)^3}H^{LL'}(\mathbf{q})\,\Pi_{LL'}(\mathbf{q},\omega)\right\},\end{aligned}\tag{30}$$

where

$$H^{LL'}(\mathbf{q}) = \int d^3x\,d^3y\,e^{-i\mathbf{q}\cdot(\mathbf{x}-\mathbf{y})}H^{LL'}(\mathbf{x},\mathbf{y}).\tag{31}$$

As can be seen from Eqs. (26) and (30), the polarized differential cross section, both for the general case and specifically for the nuclear-matter approximation, can be written as the contraction of two tensors. The first is the projectile (hadronic) tensor $H^{LL'}$, which contains all the information about the projectile and ejectile (including distortions). The other is the target (polarization) tensor $\Pi_{LL'}$, a fundamental many-body quantity that contains all the information about the target nucleus.

The simplicity in form of Eq. (30) to a large extent masks the extreme complexity of its numerical implementation. There are a number of factors that add to the numerical burden:

(i) the use of distorted waves for the projectile and ejectile wave functions;
(ii) the calculation of the polarization tensor;
(iii) the calculation of the multidimensional integrals in the hadronic tensor (the d^3x and d^3y integrals) as well as in the final evaluation of the cross section (the d^3q integral);
(iv) convergence issues of the integrals;
(v) the large number of Lorentz indices which must be contracted—25 combinations in total because $L, L' \in \{S, P, V, A, T\}$.

All these factors have greatly hampered progress in this model. However, the availability of computer packages such as MATLAB (with its powerful fitting and interpolation functions) as well as cluster computing techniques have finally made it possible to calculate the cross section in a finite and reasonable amount of time. The form of Eq. (30) allows the calculation to proceed in a modular fashion with every component easily identified and separately calculated. We can therefore easily and honestly express any assumptions that went into the calculation and profiling the calculation is greatly facilitated.

B. Amplitudes

The representation of the NN scattering matrix we employ, is the well-known SPVAT form (IA1), first formulated as the McNeil-Ray-Wallace parametrization [39,40]:

$$\begin{aligned}\hat{F} &= F_S(I_4\otimes I_4)+F_P(\gamma^5\otimes\gamma^5)+F_V(\gamma^\mu\otimes\gamma_\mu)\\ &\quad+F_A(\gamma^5\gamma^\mu\otimes\gamma^5\gamma_\mu)+F_T(\sigma^{\mu\nu}\otimes\sigma_{\mu\nu}),\end{aligned}\tag{32}$$

where the amplitudes F_L, $(L = S,\ P,\ V,\ A,\ T)$, are obtained by fitting to free NN scattering data [4], which is consistent with the basic assumption of quasielastic scattering.

Shortcomings of this representation with respect to the pion coupling, the treatment of meson exhange and the negative energy matrix elements have been pointed out in Refs. [10,23,45,47–51]; however, with the current calculation we wish to focus on the effects of distortions and target

correlations and therefore we avoid complicating this part of the model.

The IA1 amplitudes employed in this work were obtained from the IA2 representation of the scattering matrix as described in Refs. [50] and [51]. By construction the amplitudes in subclass 11 of the IA2 are identical to the SPVAT parametrization.

C. Hadronic tensor

1. Plane waves

In the plane-wave limit, the wave functions of the projectile and ejectile are given by solutions of the free Dirac equation:

$$\psi^{(+)}(\mathbf{x},\mathbf{k},\hat{i},s) = e^{i\mathbf{k}\cdot\mathbf{x}}U(\mathbf{k},\hat{i},s), \tag{33}$$

$$\psi^{(-)}(\mathbf{x},\mathbf{k}',\hat{i}',s') = e^{i\mathbf{k}'\cdot\mathbf{x}}U(\mathbf{k}',\hat{i}',s'), \tag{34}$$

where $U(\mathbf{k},\hat{i},s)$ is a four-component positive-energy Dirac spinor for spin projection s along the quantization axis $\hat{i}$. The hadronic tensor of Eq. (31) can therefore be written as

$$H^{LL'}(\mathbf{q}) = (2\pi)^3 V_N \delta(\mathbf{k}-\mathbf{k}'-\mathbf{q})[\bar{U}(\mathbf{k}',\hat{i}',s')\lambda^L U(\mathbf{k},\hat{i},s)] \times [\bar{U}(\mathbf{k},\hat{i},s)\overline{\lambda^{L'}}U(\mathbf{k}',\hat{i}',s')], \tag{35}$$

where the volume factor can be determined from the density of nuclear matter ρ_B [18] and the number of nucleons A:

$$V_N = \frac{A}{\rho_B} = \frac{3\pi^2 A}{2k_F^3}. \tag{36}$$

2. Distorted waves

The inclusion of distortion effects greatly complicates the numerical implementation because the wave functions are written in terms of partial-wave expansions. The distorted waves are solutions to the Dirac equation with scalar, timelike vector and Coulomb potentials. Because the interaction potentials are only radially dependent, a separation of the wave function into radial and angular parts is the most natural way of obtaining the solution.

The distorted wave with outgoing boundary conditions is given by [3,43,44,52]

$$\psi^{(+)}(\mathbf{x},\mathbf{k},\hat{i},s) = \frac{4\pi}{kx}\left(\frac{E(\mathbf{k})+M}{2M}\right)^{\frac{1}{2}} \sum_{ljm_l s_z} i^l e^{i\delta_{lj}} \times \left\langle l\tfrac{1}{2} m s_z \middle| j, m+s_z\right\rangle \mathcal{D}^{(\frac{1}{2})}_{s_z s}(\hat{i})\, Y^*_{lm}(\hat{k}) \times \begin{bmatrix} g_{lj}(kx)\mathcal{Y}_{lj,m+s_z}(\hat{x}) \\ i f_{2j-l,j}(kx)\mathcal{Y}_{2j-l,j,m+s_z}(\hat{x}) \end{bmatrix}, \tag{37}$$

where

(i) $x = |\mathbf{x}|$ and $k = |\mathbf{k}|$;

(ii) $\langle l\frac{1}{2} m_l m_s | j m_j\rangle$ is a Clebsch-Gordon coefficient;

(iii) $Y_{lm}(\hat{k})$ is a spherical harmonic function;

(iv) $g_{lj}(z)$ and $f_{lj}(z)$ are radial wave function solutions of Schrödinger-like radial differential equations that contain the central, spin-orbit, and Darwin potentials [3,52];

(v) $\mathcal{Y}_{lj\mu}(\hat{x})$ is a spin-spherical harmonic function written in terms of a spherical harmonic and a two-component Pauli spinor χ as

$$\mathcal{Y}_{lj\mu}(\hat{x}) = \sum_{t'_z}\left\langle l\frac{1}{2}, \mu - t'_z, t'_z \middle| j\mu\right\rangle Y_{l,\mu-t'_z}(\hat{x})\chi_{t'_z}; \tag{38}$$

(vi) the relativistic Coulomb phase shift δ_{lj} is an implicit function of the projectile and target masses, the projectile and target atomic numbers and the momentum $\mathbf{k}$. (Note that in subsequent partial-wave expansions of the projectile and ejectile wave functions we set $\delta_{lj} = 0$.)

In the specific case where $\hat{k} = \hat{z}$ and $\hat{i} = \hat{l}$ it can be written as

$$\psi^{(+)}(\mathbf{x},\mathbf{k},\hat{i},s) = \sum_{lj} A_{ljs}\begin{bmatrix} \frac{g_{lj}(kx)}{x}\mathcal{Y}_{ljs}(\hat{x}) \\ \frac{i f_{2j-l,j}(kx)}{x}\mathcal{Y}_{2j-l,js}(\hat{x}) \end{bmatrix}, \tag{39}$$

where

$$A_{ljs} = \frac{4\pi}{k}\left(\frac{E(\mathbf{k})+M}{2M}\right)^{\frac{1}{2}} i^l \left\langle l\frac{1}{2}0s \middle| js\right\rangle \left(\frac{2l+1}{4\pi}\right), \tag{40}$$

with $g_{lj}(z)$ and $f_{jl}(z)$ solutions of radial Schrödinger-like differential equations with potentials [3]. The partial-wave expansion of the ejectile can be derived using the time-reversal operator (see Appendix A):

$$\begin{aligned}\psi^{(-)}(\mathbf{x},\mathbf{k}',\hat{i}',s') &= -i(-1)^{s'-\frac{1}{2}}\mathcal{T}[\psi^{(+)}(\mathbf{x},-\mathbf{k}',\hat{i}',-s')] \\ &= \sum_{l'j'm's'_z} B_{l'j'm's'_z} \times \begin{bmatrix} \eta_{l'j'm's'_z}\frac{g^*_{l'j'}(k'x)}{x}\mathcal{Y}_{l'j',-(m'+s'_z)}(\hat{x}) \\ -i\epsilon_{l'j'm's'_z}\frac{f^*_{2j'-l',j'}(k'x)}{x}\mathcal{Y}_{2j'-l',j',-(m'+s'_z)}(\hat{x}) \end{bmatrix},\end{aligned} \tag{41}$$

where

$$B_{l'j'm's'_z} = (-i)(-1)^{s'-\frac{1}{2}}\frac{4\pi}{k'}\left(\frac{E(\mathbf{k}')+M}{2M}\right)^{\frac{1}{2}}(-1)^{s'_z+s'} i^{l'} \times \left\langle l'\frac{1}{2} m' s'_z \middle| j', m'+s'_z\right\rangle \mathcal{D}^{(\frac{1}{2})}_{-s'_z s'}(\hat{i}')\, Y_{l'm'}(\hat{k}'), \tag{42}$$

with

$$\eta_{l'j'm's'_z} = i(-1)^{m'+s'_z-j'+l'+1}, \tag{43}$$

$$\epsilon_{l'j'm's'_z} = i(-1)^{m'+s'_z+j'-l'+1}. \tag{44}$$

To calculate the hadronic current, the interaction matrix is split into 2×2 submatrices,

$$\lambda^L = \begin{bmatrix} \lambda^L_{11} & \lambda^L_{12} \\ \lambda^L_{21} & \lambda^L_{22} \end{bmatrix}, \tag{45}$$

and a partial-wave expansion is used for the exponential factor:

$$e^{-i\mathbf{q}\cdot\mathbf{x}} = 4\pi\sum_{LM}(i^L)^* j_L(qx)Y_{LM}(\hat{q})Y^*_{LM}(\hat{x}). \tag{46}$$

This allows the hadronic current to be written as

$$H^L(\mathbf{q}) = I_{11} + I_{12} + I_{21} + I_{22}, \tag{47}$$

where

$$I_{11} = \sum_{lj}\sum_{l'j'm's'_z} 4\pi A_{ljs} B^*_{l'j'm's'_z} \eta^*_{l'j'm's'_z} \sum_{LM} (i^L)^* Y_{LM}(\mathbf{q}) \left\{ \int dr\; j_L(qr)\, g_{lj}(kr)\, g_{l'j'}(k'r) \right\} \sum_{t_z t'_z} \left\langle l \frac{1}{2}, s - t_z, t_z \middle| js \right\rangle$$
$$\times \left\langle l' \frac{1}{2}, -m' - s'_z - t'_z, t'_z \middle| j', -m' - s'_z \right\rangle [\chi^\dagger_{t'_z} \lambda^L_{11} \chi_{t_z}] G(l, s - t_z | l', -m' - s'_z - t'_z | LM), \tag{48}$$

$$I_{12} = \sum_{lj}\sum_{l'j'm's'_z} 4\pi A_{ljs} B^*_{l'j'm's'_z} \left(i\eta^*_{l'j'm's'_z}\right) \sum_{LM} (i^L)^* Y_{LM}(\mathbf{q}) \left\{ \int dr\; j_L(qr)\, f_{2j-l,j}(kr)\, g_{l'j'}(k'r) \right\} \sum_{t_z t'_z} \left\langle 2j - l, \frac{1}{2}, s - t_z, t_z \middle| js \right\rangle$$
$$\times \left\langle l' \frac{1}{2}, -m' - s'_z - t'_z, t'_z \middle| j', -m' - s'_z \right\rangle [\chi^\dagger_{t'_z} \lambda^L_{12} \chi_{t_z}] G(2j - l, s - t_z | l', -m' - s'_z - t'_z | LM), \tag{49}$$

$$I_{21} = \sum_{lj}\sum_{l'j'm's'_z} 4\pi A_{ljs} B^*_{l'j'm's'_z} \left(-i\epsilon^*_{l'j'm's'_z}\right) \sum_{LM} (i^L)^* Y_{LM}(\mathbf{q}) \left\{ \int dr\; j_L(qr)\, g_{lj}(kr)\, f_{2j'-l',j'}(k'r) \right\} \sum_{t_z t'_z} \left\langle l, \frac{1}{2}, s - t_z, t_z \middle| js \right\rangle$$
$$\times \left\langle 2j' - l' \frac{1}{2}, -m' - s'_z - t'_z, t'_z \middle| j', -m' - s'_z \right\rangle [\chi^\dagger_{t'_z} \lambda^L_{21} \chi_{t_z}] G(l, s - t_z | 2j' - l', -m' - s'_z - t'_z | LM), \tag{50}$$

$$I_{22} = \sum_{lj}\sum_{l'j'm's'_z} 4\pi A_{ljs} B^*_{l'j'm's'_z} \epsilon^*_{l'j'm's'_z} \sum_{LM} (i^L)^* Y_{LM}(\mathbf{q}) \left\{ \int dr\; j_L(qr)\, f_{2j-l,j}(kr)\, f_{2j'-l',j'}(k'r) \right\} \sum_{t_z t'_z} \left\langle 2j - l, \frac{1}{2}, s - t_z, t_z \middle| js \right\rangle$$
$$\times \left\langle 2j' - l' \frac{1}{2}, -m' - s'_z - t'_z, t'_z \middle| j', -m' - s'_z \right\rangle [\chi^\dagger_{t'_z} \lambda^L_{22} \chi_{t_z}] G(2j - l, s - t_z | 2j' - l', -m' - s'_z - t'_z | LM). \tag{51}$$

Note that here the angular integral has been incorporated into a Gaunt coefficient. For Eq. (48) this would be given by

$$G(l, s - t_z | l', -m' - s'_z - t'_z | LM)| = \int d\Omega\, Y_{l,s-t_z}(\hat{x})\, Y^*_{l',-m'-s'_z-t'_z}(\hat{x})\, Y^*_{LM}(\hat{x}). \tag{52}$$

and selection rules of these coefficients [53] would imply that

$$\left|l - l'\right| \leqslant L \leqslant (l + l'), \quad M = s + s'_z + m' - t_z + t'_z. \tag{53}$$

D. Polarization tensor

1. Lowest order

The polarization is evaluated in the Hartree approximation where the nuclear ground state is the self-consistent MFT ground state [18,54] and, using Wick's theorem [3,28], the polarization tensor (shown in Fig. 2) can be written as

$$\Pi^{LL'}(q) = -i \int \frac{d^4k}{(2\pi)^4} \mathrm{Tr}[\lambda^L G^H(k) \overline{\lambda^{L'}} G^H(k + q)]. \tag{54}$$

Here the nucleon propagator can be written in terms of Feynman (F) and density-dependent (D) pieces

$$G^H(k) = G_F(k) + G_D(k), \tag{55}$$

$$G_F(k) = (\bar{\not{k}} + M^*) \left[\frac{1}{\bar{k}^2 - M^{*2} + i\epsilon} \right], \tag{56}$$

$$G_D(k) = (\bar{\not{k}} + M^*) \left[\frac{i\pi}{E^*_k} \delta(\bar{k}^0 - E^*_k) \theta(k_F - |\mathbf{k}|) \theta(\bar{k}^0) \right], \tag{57}$$

$$\bar{k}^\mu = (k^0 - g_V V^0, \mathbf{k}), \tag{58}$$

$$E^*_k = \sqrt{\mathbf{k}^2 + M^{*2}}, \tag{59}$$

$$M^* = M - g_s \phi_0. \tag{60}$$

This allows the polarization tensor of Eq. (54) to be written as

$$\Pi^{LL'}(q) = \Pi^{LL'}_{FF}(q) + \Pi^{LL'}_{D}(q), \tag{61}$$

where

$$\Pi^{LL'}_{FF}(q) = \int \frac{d^4k}{(2\pi)^4} \frac{-i\mathcal{T}^{LL'}(k, k + q)}{[\bar{k}^2 - M^{*2} + i\epsilon][(\bar{k} + q)^2 - M^{*2} + i\epsilon]}, \tag{62}$$

and

$$\Pi^{LL'}_{D}(q) = \int \frac{d^4k}{(2\pi)^4} \frac{\pi\theta(k_F - |\mathbf{k}|)\theta(\bar{k}^0)}{E^*_k} \delta(\bar{k}^0 - E^*_k) \left\{ \frac{\mathcal{T}^{LL'}(k, k + q)}{(\bar{k} + q)^2 - M^{*2} + i\epsilon} + \frac{\mathcal{T}^{LL'}(k - q, k)}{(\bar{k} - q)^2 - M^{*2} + i\epsilon} \right\}$$
$$+ i \int \frac{d^4k}{(2\pi)^4} \frac{\pi^2\theta(k_F - |\mathbf{k}|)\theta(k_F - |\mathbf{k} + \mathbf{q}|)\theta(\bar{k}^0)\theta(\bar{k}^0 + q^0)}{E^*_k E^*_{k+q}} \delta(\bar{k}^0 - E^*_k) \delta(\bar{k}^0 + q^0 - E^*_{k+q}) \mathcal{T}^{LL'}(k, k + q), \tag{63}$$

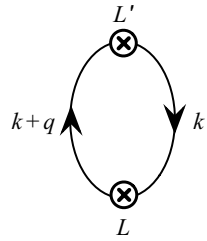

FIG. 2. Lowest-order (Hartree) polarization where $L, L' \in \{S, P, V, A, T\}$ [2].

with

$$\mathcal{T}^{LL'}(k, k+q) = \mathrm{Tr}[\lambda^L G^H(k)\overline{\lambda^{L'}} G^H(k+q)], \quad (64)$$

$$\mathcal{T}^{LL'}(k-q, k) = \mathrm{Tr}[\lambda^L G^H(k-q)\overline{\lambda^{L'}} G^H(k)]. \quad (65)$$

Here Π_D consists of three pieces: Π_{FD}, Π_{DF}, and Π_{DD}. These terms originate from the polarization of the Fermi sea. The first two contain only one density-dependent contribution and describe particle-hole excitations and the Pauli blocking of nucleon-antinucleon excitations. Π^{DD} cancels Pauli-forbidden particle-hole excitations contained in these terms [21].

Π_{FF} (also known as the vacuum polarization) originates from the polarization of the Dirac sea. It is explicitly density-independent although implicitly it does depend on the density owing to the presence of M^*. It describes $N\bar{N}$ excitations, is divergent and has to be regularized and renormalized [18,21]. The imaginary part of this piece vanishes for spacelike momentum transfers and where $q_\mu^2 < 4M^{*2}$ (the threshold for nucleon-antinucleon production). The real part of Π_{FF} describes the virtual excitation of nucleon-antinucleon pairs. In a calculation based on the MFT ground state, where the vacuum contributions to the self-energies are ignored, it is consistent to omit the vacuum polarization completely [21,55]. Note that the Pauli-blocking of nucleon-antinucleon pairs present in Π_D is retained in the MFT approximation, among others, to satisfy current conservation [22,25,55].

Because both the real and the imaginary parts of Π_D contribute to the polarization tensor we now turn to the calculation of these quantities.

In principle, polarization tensors of all 25 LL' combinations need to be calculated. This process is systematized by arranging the polarization tensors according to the number of Lorentz indices as determined by L and L' from zeroth-order tensors up to fourth order. Using this scheme, contributions from different LL' channels to the cross section can be determined by successively calculating increasingly complicated expressions and tensor contractions.

In Eq. (63) the integral over k^0 can be performed by making a shift of variables from k^0 to $\bar{k}^0$. Note that this eliminates the constant vector potential of the mean field leaving the only traces of the relativistic ground-state dynamics in the effective mass [2].

The real part of $\Pi_D^{LL'}$ is obtained by applying the Cauchy principal value theorem

$$\frac{1}{\omega \pm i\epsilon} = \mathcal{P}(\omega) \mp i\pi\delta(\omega) \quad (66)$$

and can be written as

$$\mathrm{Re}\{\Pi_D^{LL'}\} = \frac{1}{16\pi^3}\mathcal{P}\int_0^{k_F} d|\mathbf{k}|\,\frac{\mathbf{k}^2}{E_k^*} I_\Omega^{LL'}(k, q), \quad (67)$$

where the angular part, $I_\Omega^{LL'}(k, q)$, can be calculated analytically (typical expressions are shown in Appendix B).

Similarly, the imaginary part is given by

$$\begin{aligned}\mathrm{Im}\{\Pi_D^{LL'}\} = -\frac{1}{16\pi|\mathbf{q}|}\int dE_k^*\theta(E_F - E_k^*) \\ \times \theta(E_k^* - M^*)\theta(-E_F + E_k^* + q^0) \\ \times \theta\left(-E_k^{*2}q_\mu^2 - M^{*2}\mathbf{q}^2 - E_k^* q^0 q_\mu^2 - \frac{q_\mu^4}{4}\right) \\ \times \mathcal{T}^{LL'}(k, k+q)_{\bar{k}^0 = E_k^*} \quad (68)\end{aligned}$$

and can be solved analytically for every trace (typical expressions are shown in Appendix B). Note that here the step functions impose limits on the integral [3,56,57].

In general, the integrals over the traces and the resultant tensor structures of the polarization tensors are more manageable in a coordinate system where $q^\mu = (\omega, 0, 0, |\mathbf{q}|)$. Because the trace expressions are invariant under spatial rotation, the polarization tensors in the original coordinate system, as specified by the integration variable $\mathbf{q}$, are then obtained by applying a rotation operator

$$R(\alpha, \beta) = R_z(\alpha)R_y(\beta), \quad (69)$$

where the Euler angles have been identified as the angles of $\mathbf{q}$:

$$\beta = \theta_q, \quad \alpha = \phi_q. \quad (70)$$

2. RPA

In the lowest-order Hartree approximation the residual interaction of the particle-hole pair created in the nucleus by the external probe is neglected [35]. The RPA takes this interaction into account by summing the uncorrelated Hartree responses (ring diagrams) to all orders [33]. The particle-hole or nucleon-antinucleon pair that is excited in the nucleus travels through the many-body medium and interacts with the self-consistent mean field. Because the fitting of bulk nuclear properties constrains only isoscalar particle-hole interactions significantly [22], we restrict our current calculation to isoscalar excitations.

In the context of the interacting meson-nucleon model (QHD) this infinite summation is accomplished by calculating the medium-modified meson propagators as shown in Fig. 3. At present, only medium-modification of isoscalar σ and ω mesons are considered and therefore X and Y is S or V as determined by the QHD-I Lagrangian where scalar σ and vector ω meson have bare scalar and vector couplings. The complete RPA polarization tensor is obtained by adding this effect to the lowest-order polarization tensor for every LL' channel as shown. This is reflected in the matrix equation

$$\tilde{\Pi}^{LL'}(q) = \Pi^{LL'}(q) + \Pi^{Li}(q)\,\tilde{D}_{ij}(q)\,\Pi^{jL'}(q), \quad (71)$$

where $\tilde{D}$ is known as the medium-modified interaction [2] and can be viewed as the modification of the meson propagators

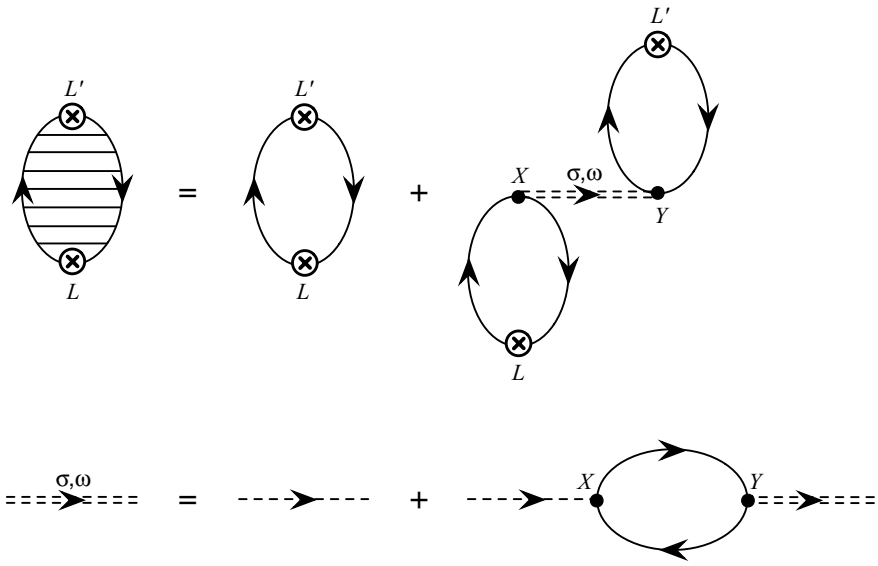

FIG. 3. Diagrammatic representation of the RPA summation [2] and the Dyson's equation for the isoscalar interaction.

owing to coupling to nuclear excitations [55]. Here Latin indices i and j denote the elementary coupling of a nucleon to a meson [i.e., σ ($i = -1$) and ω ($i = 0,\ 1,\ 2,\ 3$)]. $\tilde{D}$ contains all the RPA dynamics and satisfies the following Dyson's equation (see Fig. 3):

$$\tilde{D}_{ij}(q) = D^0_{ij}(q) + D^0_{ik}(q)\,\Pi^{kl}_0(q)\,\tilde{D}_{lj}(q), \tag{72}$$

or as the solution of a 5×5 matrix equation,

$$\tilde{D} = (1 - D^0\Pi_0)^{-1} D^0, \tag{73}$$

where the free-space interaction matrix D^0 is given by

$$D^0_{ij} = \begin{bmatrix} D^{(\sigma)} & 0 \\ 0 & D^{(\omega)}_{\alpha\beta} \end{bmatrix}, \tag{74}$$

with

$$D^{(\sigma)}(q) = g_s^2 \Delta^0(q) = \frac{g_s^2}{q_\mu^2 - m_s^2}, \tag{75}$$

$$D^{(\omega)}_{\alpha\beta}(q) = \left(-g_{\alpha\beta} + \frac{q_\alpha q_\beta}{m_v^2}\right) \frac{g_v^2}{q_\mu^2 - m_v^2}. \tag{76}$$

Note that in nuclear matter the ω meson always couples to a conserved baryon current (i.e., $q_\mu \Pi^{\mu\nu} = 0$) and the $q_\alpha q_\beta$ term will therefore not contribute to the RPA reponse [24,55]. Because the elementary coupling of the nucleon to the σ and ω mesons have been chosen as the bare scalar and vector couplings and mixing of scalar and vector polarizations can occur in the medium [54], the mixed Hartree polarization matrix Π_0 used in the evaluation of the medium-modified interaction of Eq. (73) is given by

$$\Pi^{ij}_0 = \begin{bmatrix} \Pi^{SS} & \Pi^{SV} \\ \Pi^{VS} & \Pi^{VV} \end{bmatrix}, \tag{77}$$

where the individual Hartree components are calculated according to the procedure outlined in Sec. II D 1.

Analytical expressions for the components of $\tilde{D}$ in nuclear matter are shown in Appendix C.

III. CALCULATIONAL PROCEDURE

In the case of $(\vec{p}, \vec{p}\,')$ scattering, the amplitudes are half isoscalar and half isovector. This implies that the cross section of Eq. (30) can be written as

$$\frac{d\sigma}{dE'\,d\Omega'} = -\frac{1}{\pi} K\,\mathrm{Im}\left\{ \sum_{L,L'=S}^{T} \left(\frac{1}{2}F_L^{\mathrm{isos}} + \frac{1}{2}F_L^{\mathrm{isov}}\right) \times \left(\frac{1}{2}F_{L'}^{\mathrm{isos}\,*} + \frac{1}{2}F_{L'}^{\mathrm{isov}\,*}\right) \times \int \frac{d^3q}{(2\pi)^3}\, H^{LL'}(\mathbf{q})\,\Pi_{LL'}(\mathbf{q},\omega) \right\}. \tag{78}$$

In the Walecka model (QHD-I) nucleons interact through the exchange of isoscalar mesons only and the nucleon propagators do not have isovector components [35]. The cross section can therefore be written in terms of decoupled isoscalar and isovector channels. Because our model at present only takes isoscalar correlations into account, only the isoscalar channel is affected and the polarized double differential cross section with and without isoscalar RPA corrections is calculated as

$$\frac{d\sigma}{dE'\,d\Omega'} = -\frac{1}{\pi}\mathcal{K}\,\mathrm{Im}\left\{ \sum_{L,L'=S}^{T} \left[\frac{1}{4}F_L^{\mathrm{isos}} F_{L'}^{\mathrm{isos}\,*} \int \frac{d^3q}{(2\pi)^3} \times H^{LL'}(\mathbf{q})\Pi_{LL'}(\mathbf{q},\omega) + \frac{1}{4}F_L^{\mathrm{isov}} F_{L'}^{\mathrm{isov}\,*} \times \int \frac{d^3q}{(2\pi)^3}\, H^{LL'}(\mathbf{q})\,\Pi_{LL'}(\mathbf{q},\omega) \right] \right\}, \tag{79}$$

$$\left(\frac{d\sigma}{dE'\,d\Omega'}\right)_{\mathrm{RPA}} = -\frac{1}{\pi}\mathcal{K}\,\mathrm{Im}\left\{ \sum_{L,L'=S}^{T} \left[\frac{1}{4}F_L^{\mathrm{isos}} F_{L'}^{\mathrm{isos}\,*} \int \frac{d^3q}{(2\pi)^3} \times H^{LL'}(\mathbf{q})\tilde{\Pi}_{LL'}(\mathbf{q},\omega) + \frac{1}{4}F_L^{\mathrm{isov}} F_{L'}^{\mathrm{isov}\,*} \times \int \frac{d^3q}{(2\pi)^3}\, H^{LL'}(\mathbf{q})\,\Pi_{LL'}(\mathbf{q},\omega) \right] \right\}. \tag{80}$$

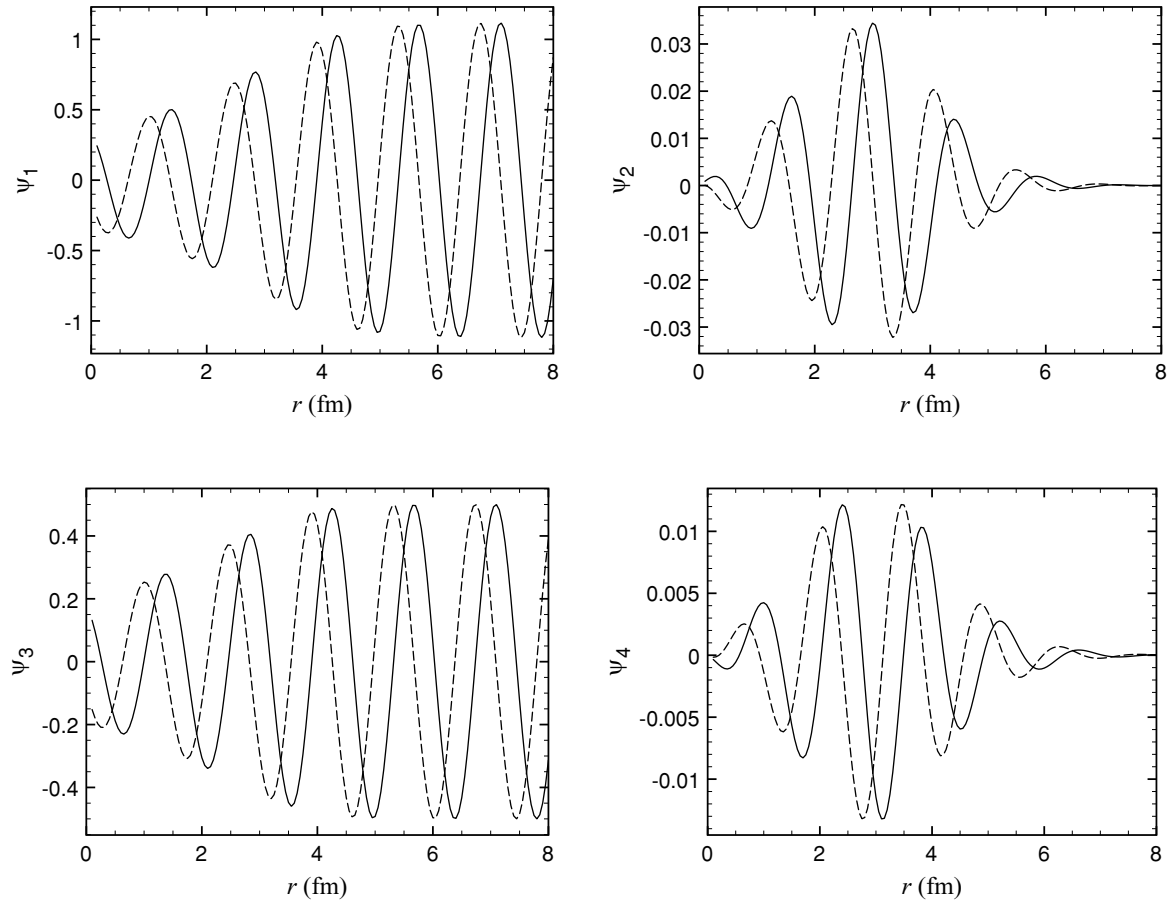

FIG. 4. Real (solid) and imaginary (dashed) parts of the four components of the Dirac distorted wave as a function of radius. This wave was generated for $T_{\rm lab} = 500$ MeV, $(\hat{i}, s) = (\hat{l}, 1/2)$ and $l_{\rm max} = 60$ for ^{40}Ca. θ and ϕ were arbitrarily chosen as $\pi/1.23$ and $2\pi/5.43$, respectively. Beyond $r = 8$ fm the plane-wave behavior is restored.

A. Distorted wave cross section

The behavior of the distorted waves for different values of $l_{\rm max}$ can be seen in Figs. 4 and 5. Here they have been generated according to Eq. (39) for zero Coulomb distortions ($\delta_{lj} = 0$) as described in Ref. [3] using the optical potential of Ref. [15]. Beyond $l_{\rm max} = 60$ they do not change significantly; however, owing to constraints in computational resources, we set $l_{\rm max} = l'_{\rm max} = 30$ for our RDWIA calculation. As can be seen in Fig. 5, the first, second, and third components of the distorted waves are already in good quantitative agreement with the $l_{\rm max} = 60$ results. From these figures it is evident that the effect of distortions is an attenuation of the plane wave. Note that beyond $r = 8$ fm the plane-wave behavior is restored (for ^{40}Ca).

The numerical complexity of the calculation of the cross section in the distorted wave case cannot be overemphasized. Strictly speaking, the integral is over nine dimensions, namely, d^3x, d^3y, and d^3q. The primary reason for the numerical complexity is the use of the partial-wave expansion of the distorted waves and convergence issues of the multidimensional integrals. A brute-force approach with Gaussian quadrature and Monte Carlo methods proved cumbersome and did, indeed, lead to poor convergence.

In Eq. (48) we showed that the multidimensional spatial integral can be reduced to a one-dimensional radial integral and the two-dimensional angular integrals which reduce to the so-called Gaunt coefficients. These latter quantities exhibit a number of symmetries which aid in the evaluation of the hadronic tensor. Nonetheless, even their calculation is a highly nontrivial matter. We made use of the method of Rash and Yu [58,59] to generate the Gaunt coefficients in MATHEMATICA and implement them in the cross-section calculation in FORTRAN. These coefficients are invariant under any permutation of l, m pairs as well as spatial reflection $(m_1, m_2, m_3 \to -m_1, -m_2, -m_3)$. In conjunction with the selection rules this implies that they can be generated for $l_1 \geqslant l_2 \geqslant l_3$, $m_3 \geqslant 0$, $-l_2 \leqslant m_2 \leqslant \min(l_1 - m_3, l_2)$, and $m_1 = -m_2 - m_3$. In FORTRAN they are stored in an array of pointers indexed by l_1, l_2, l_3, m_3 according to

$$\begin{aligned} c &= \sum_{i=0}^{l_1}\sum_{j=0}^{i}\sum_{k=0}^{j} k + \sum_{j}^{l_2}\sum_{k=0}^{j} k + \sum_{k=0}^{l_3} k + m_3 + 1 \\ &= \frac{1}{24} l_1 \{6 + l_1 [11 + l_1 (6 + l_1)]\} + \frac{1}{6} l_2 [2 + l_2 (3 + l_2)] \\ &\quad + \frac{1}{2} l_3 (l_3 + 1) + m_3 + 1 \end{aligned} \tag{81}$$

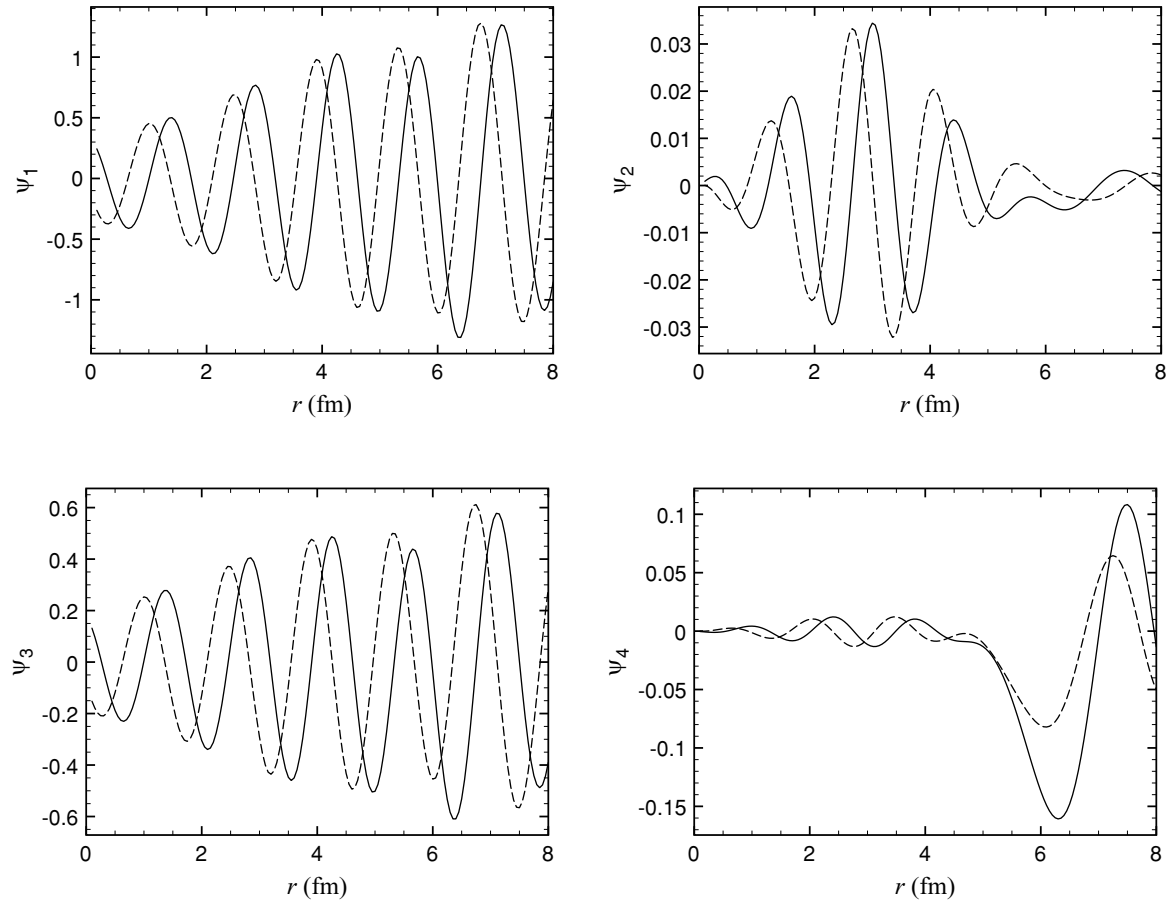

FIG. 5. Real (solid) and imaginary (dashed) parts of the four components of the Dirac distorted wave as a function of radius. This wave was generated for $T_{\rm lab} = 500$ MeV, $(\hat{i}, s) = (\hat{l}, 1/2)$ and $l_{\rm max} = 30$ for ^{40}Ca. θ and ϕ were arbitrarily chosen as $\pi/1.23$ and $2\pi/5.43$, respectively. Beyond $r = 8$ fm the plane-wave behavior is restored.

and each of these pointers points to a vector indexed by m_2 according to

$$i = m_2 + l_2 + 1. \tag{82}$$

Note that computation time and storage space needed can be greatly reduced if the selection rules are hard coded. In the end, approximately 400 MB of storage space was required and the once-off calculation of all coefficients was completed in 24 h on a desktop PC with an Intel Core 2 Duo processor and 4 GB of RAM.

The radial integral was evaluated using the standard Gaussian integration subroutine, *gauleg,* fully discussed on page 145 of Ref. [60]. The difficulty here was attributable to the fact that the distorted upper and lower radial wave functions, g_{lj} and f_{lj}, respectively, are not analytical expressions but are stored in large arrays for the different values of l and j and the kinematical quantity $z = kr$ or $z = k'r$. Convergence for these integrals were obtained for 30 Gaussian grid points for an upper limit of $r = 8$ fm (the range of the nuclear potential for ^{40}Ca).

The method of separating the spatial integrals into radial and angular parts does not work for the momentum integral (d^3q integral) because the polarization tensor does not necessarily exhibit such symmetries. We therefore now face the dilemma of having to calculate a three-dimensional integral where the integrand is a highly complex quantity with a strong oscillatory nature. A number of integration methods [61–64] were explored for this problem but all turned out to be of little practical use. This is where the powerful interpolation and fitting procedures of MATLAB became a primary calculational tool. The key point to note is that the three-dimensional integral d^3q can be written as $d^3q = d|\mathbf{q}|\, d\Omega_q$. A straightforward application of the Gaussian integration method would then require N^3 integration points where N is the number of Gaussian integration points needed for one dimension. We can, however, perform the two-dimensional integral over (say) the angular part (N^2 Gaussian grid points) for a certain set of $|\mathbf{q}|$ values, by defining the function $f(|\mathbf{q}|, \omega)$ as

$$\begin{aligned}\frac{d\sigma}{dE'\,d\Omega'} &= \int_{q_{\rm min}}^{q_{\rm max}} d|\mathbf{q}|\, f(|\mathbf{q}|, \omega) \\ &= \int_{q_{\rm min}}^{q_{\rm max}} d|\mathbf{q}| \Bigg[-\frac{|\mathbf{q}|^2}{8\pi^4} \mathcal{K}\, {\rm Im} \Bigg\{ \sum_{L,L'=S}^{T} F_L(T_{\rm lab}, |\mathbf{q}|) \\ &\quad \times F^*_{L'}(T_{\rm lab}, |\mathbf{q}|) \int d\phi_q\, d\theta_q \sin\theta_q H^{LL'}(|\mathbf{q}|, \theta_q, \phi_q) \\ &\quad \times \Pi_{LL'}(|\mathbf{q}|, \theta_q, \phi_q, \omega) \Bigg\} \Bigg]. \end{aligned} \tag{83}$$

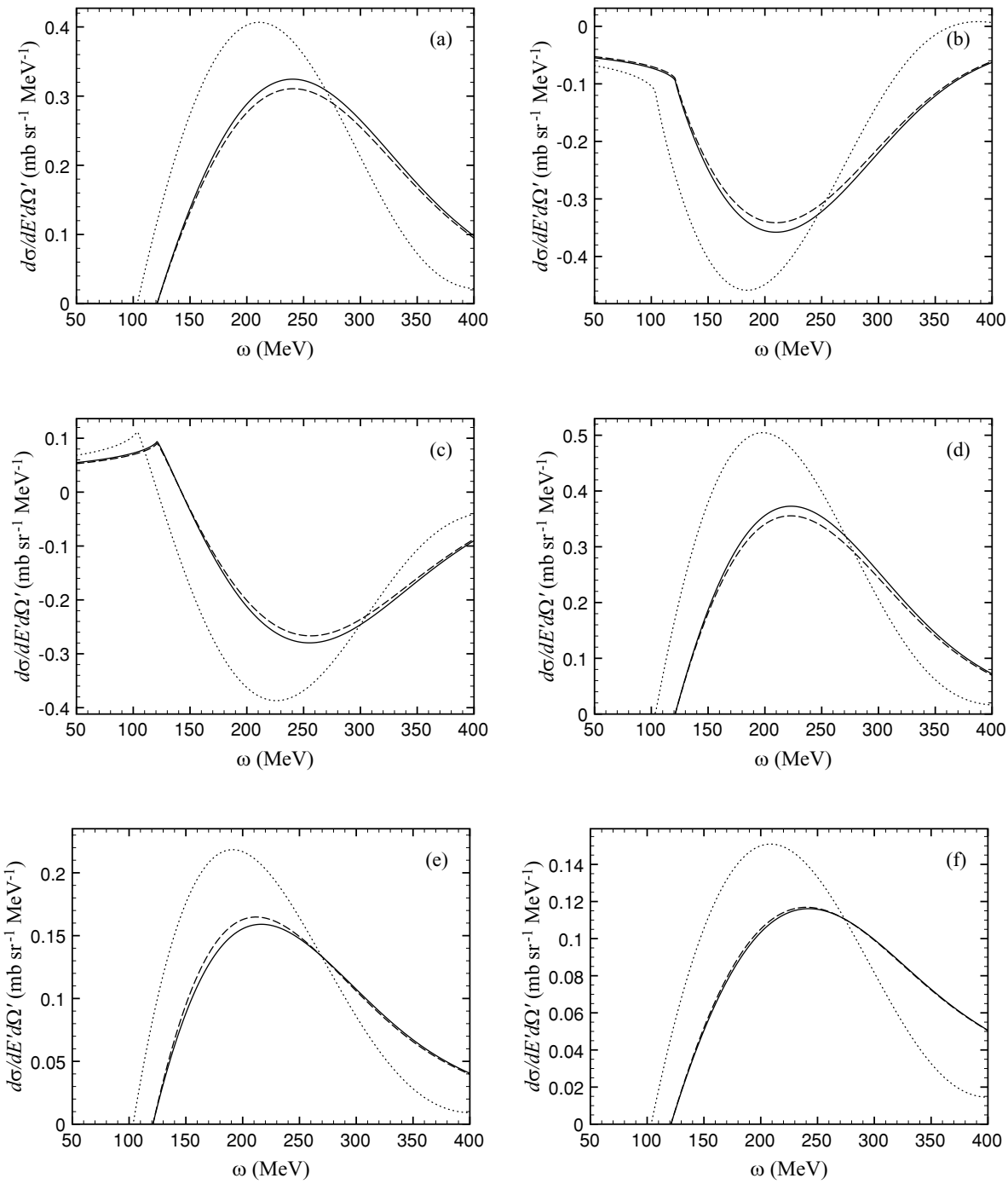

FIG. 6. Plane-wave polarized double differential cross sections for $LL' =$ (a) SS, (b) SV, (c) VS, (d) VV, (e) AA, and (f) TT for the reaction ^{40}Ca($\vec{p}$, $\vec{p}\,'$). In all figures the solid line indicates the MFT (Hartree), the dashed line the MFT (RPA), and the dotted line the $M^* = M$ (Hartree) calculations. Here $T_{\rm lab} = 500$ MeV, $k_F = 0.955$ fm^{-1}, $(\hat{\imath}, s) = (\hat{l}, 1/2)$, $(\hat{\imath}', s') = (\hat{l}', 1/2)$, and $\theta_{\rm c.m.} = 40^\circ$.

Because this function is now defined on a grid of $|\mathbf{q}|$ values we can use an interpolation scheme (be it analytical or a spline method) to calculate $f(|\mathbf{q}|, \omega)$ for any value of $|\mathbf{q}|$. This function is fairly well-behaved and the remaining one-dimensional integral can be performed numerically for a low number of grid points. The whole calculational procedure can be automated with the *cftool* interpolation and fitting package in MATLAB. Using this method we have devised a novel calculational procedure to evaluate the distorted wave cross section in a reasonable time. For example, the calculation of the function $f(|\mathbf{q}|, \omega)$ for 40^2 grid points (in the angular space) and one grid point in the $|\mathbf{q}|$ space takes approximately four days on a desktop PC with a 3-GHz Intel Pentium 4 processor and 2 GB of RAM. At this point we employ cluster computing methods, where each cluster PC calculates the cross section for different $|\mathbf{q}|$ and ω values. The distribution of the

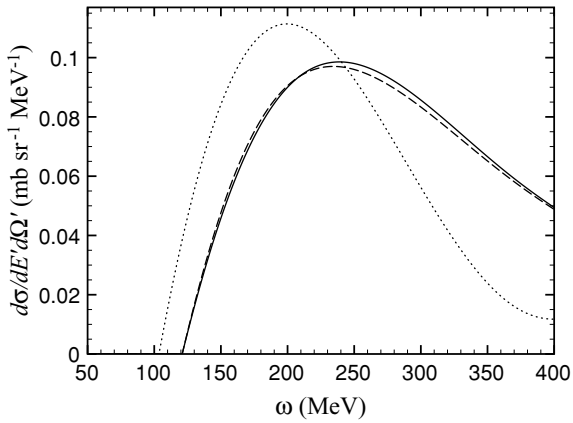

FIG. 7. Plane-wave polarized double differential cross sections summed over all LL' combinations for the reaction ^{40}Ca($\vec{p}$, $\vec{p}\,'$). The solid line indicates the MFT (Hartree), the dashed line the MFT (RPA), and the dotted line the $M^* = M$ (Hartree) calculations. Here $T_{\rm lab} = 500$ MeV, $k_F = 0.955$ fm^{-1}, $(\hat{\imath}, s) = (\hat{l}, 1/2)$, $(\hat{\imath}', s') = (\hat{l}', 1/2)$, and $\theta_{\rm c.m.} = 40^\circ$.

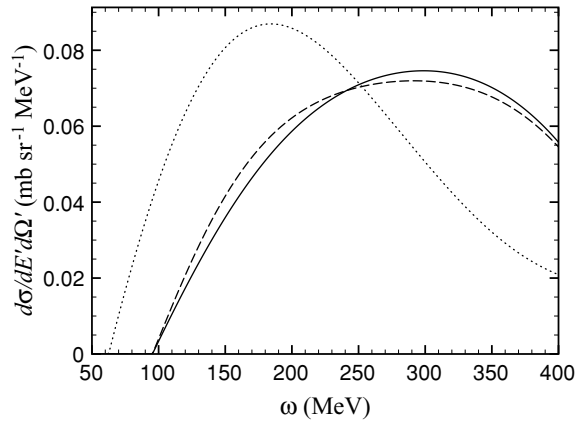

FIG. 8. Plane-wave polarized double differential cross sections summed over all LL' combinations for the reaction ^{40}Ca($\vec{p}$, $\vec{p}\,'$). The solid line indicates the MFT (Hartree), the dashed line the MFT (RPA), and the dotted line the $M^* = M$ (Hartree) calculations. Here $T_{\rm lab} = 500$ MeV, $k_F = 1.3$ fm^{-1}, $(\hat{\imath}, s) = (\hat{l}, 1/2)$, $(\hat{\imath}', s') = (\hat{l}', 1/2)$, and $\theta_{\rm c.m.} = 40^\circ$.

calculational burden across the cluster PCs enables one to obtain the distorted wave cross section as a function of ω. This emphasizes, once again, the computational difficulty in the evaluation of the distorted wave cross section. However, the whole procedure can be automated and human intervention is only required at the start and at the end to collect the results. The accuracy of the fitting procedure was verified for the plane-wave cross section by explicitly performing the d^3q integral and subsequent comparison.

From plane-wave and distorted wave interpolation plot it was found that a $40^2 \times 11$ fiting procedure (40^2 for $d\Omega$ and 11 for $d|\mathbf{q}|$) is sufficient to interpolate the $f(|\mathbf{q}|, \omega)$ reliably owing to its relative smoothness if spline interpolants are used.

IV. RESULTS

A. Plane-wave cross sections

LL' contributions to the cross section were calculated using $k_F = 0.955$ fm^{-1} for ^{40}Ca($\vec{p}$, $\vec{p}\,'$) at a projectile energy $T_{\rm lab} = 500$ MeV [23] (parameter set shown in Table I). This is lower than the Fermi momentum at saturation density ($k_F = 1.3$ fm^{-1}) because quasielastic proton scattering peaks at the nuclear surface [4,23] owing to a decrease in transmission through the inner nucleus at higher beam energies. For comparison, results were also generated for $k_F = 1.3$ fm^{-1}. All cross-section results are plotted in the center-of-mass frame. It should be noted that these calculations are presented to exhibit the behavior of the model and gauge the effects of different model-components. Experimental data for all center-of-mass angles for which calculations are presented might not necessarily exhibit pure single-step behavior.

Figure 6 shows the contributions from the largest LL' combinations to the cross section for $k_F = 0.955$ fm^{-1}. Even though the shape and sign of some of these curves may seem unphysical when (erroneously) interpreted as measurable cross sections in their own right, it is important to note that these appearances are a result of the parametrization in terms of S, P, V, A, and T and that the final measurable cross section (the sum of the LL' contributions) shown in Fig. 7 is, in fact, consistently positive and exhibits the familiar shape of the quasielastic peak. It is, however, interesting to note that the largest effect on the cross section arises from these combinations.

The result for the polarized double differential cross section summed over all LL' (Fig. 7) shows a clear shift to higher energy transfer ($\omega_{\rm peak} \sim 1/2M^*$), a decrease in the magnitude, and a widening ($\Delta\omega \sim 1/M^*$) of the quasielastic peak associated with a decrease in the mass of the target nucleon when the $M = M^*$ and MFT calculations are compared. This becomes especially evident when comparing the lower density ($k_F = 0.955$ fm^{-1}, $M^* = 0.817M$) and saturation density ($k_F = 1.3$ fm^{-1}, $M^* = 0.541M$) curves (Figs. 7 and 8). Figure 9 shows how the cross section shifts to higher energy transfer and decreases with increasing scattering angles. These phenomena are consistent with the general features of RIA + RMF models for quasielastic scattering of leptons and hadrons [1,2,23,26,34,36].

In addition, the RPA correction further tends to reduce the magnitude of the quasielastic peak in the MFT result owing to the attractive particle-hole interaction [26]. This

TABLE I. Parameter values and effective masses for different values of k_F [21]. These values are used in the calculation of the cross sections.

Model	g_s^2	g_v^2	m_s (MeV)	m_v (MeV)	M^*/M (1.3 fm^{-1})	M^*/M (0.955 fm^{-1})
MFT	109.626	190.431	520	783	0.541	0.817

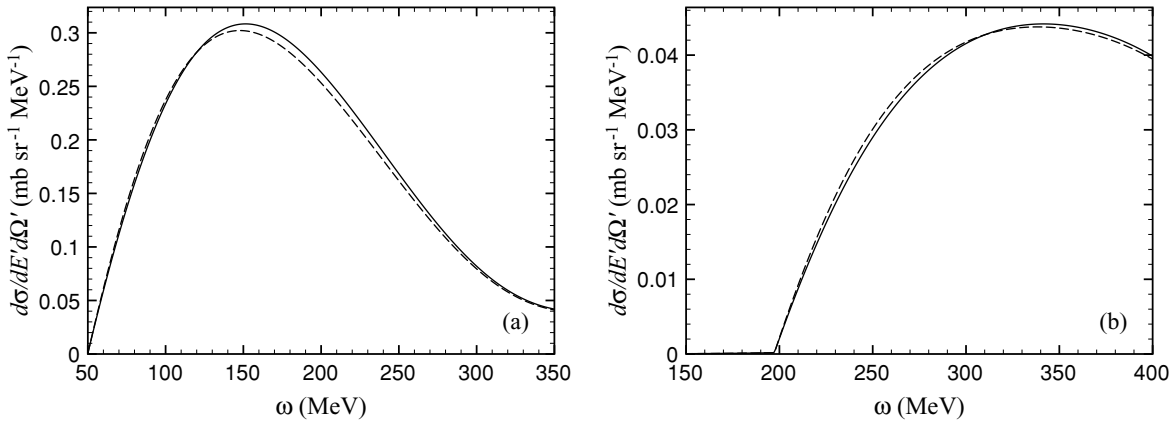

FIG. 9. Plane-wave polarized double differential cross sections summed over all LL' combinations for (a) $\theta_{\text{c.m.}} = 30^\circ$ and (b) $\theta_{\text{c.m.}} = 50^\circ$ for the reaction ^{40}Ca$(\vec{p}, \vec{p}\,')$. In all figures the solid line indicates the MFT (Hartree) and the dashed line the MFT (RPA) calculations. Here $T_{\text{lab}} = 500$ MeV, $k_F = 0.955$ fm^{-1}, $(\hat{i}, s) = (\hat{l}, 1/2)$, and $(\hat{i}', s') = (\hat{l}', 1/2)$.

effect increases with target density, as is evident from the saturation density results shown in Fig. 8. In addition, Fig. 9 shows that the isoscalar correlations become slightly stronger at lower scattering angles (for similar values of the energy transfer) where momentum transfer is lower. Reference [21] ascribes this to the damping of meson propagators at large $|\mathbf{q}|$. The impact of isoscalar correlations does not seem to be very large for this specific reaction and kinematics. We comment on this in the Conclusion.

B. Distorted wave cross section

From the result for $LL' = SS$ shown in Fig. 10 it is clear that the RDWIA cross section is quenched relative to the RPWIA, even at $l_{\text{max}} = 30$, and that the peak is shifted slightly.

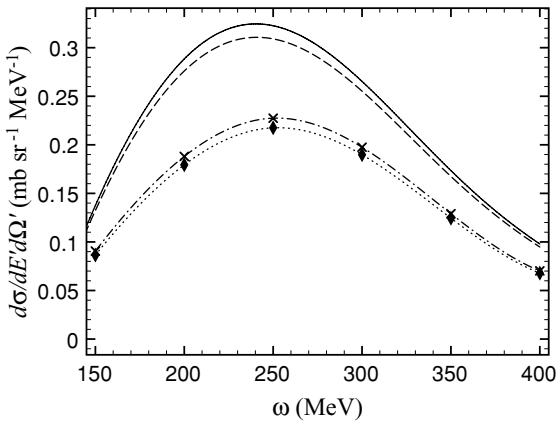

FIG. 10. Comparison of the RPWIA and RDWIA polarized double differential cross sections for $LL' = SS$ for the reaction ^{40}Ca$(\vec{p}, \vec{p}\,')$. The solid (dashed) line indicates the RPWIA and lowest-order MFT (MFT + RPA) result. The dashed-dotted (dotted) line indicates the RDWIA and lowest-order MFT (MFT + RPA) result. Crosses and diamonds indicate the result of the $40^2 \times 11$ fitting calculation for every value of ω. Here $T_{\text{lab}} = 500$ MeV, $k_F = 0.955$ fm^{-1}, $(\hat{i}, s) = (\hat{l}, 1/2)$, $(\hat{i}', s') = (\hat{l}', 1/2)$, $\theta_{\text{c.m.}} = 40^\circ$, and $l_{\text{max}} = 30$.

The inclusion of isoscalar RPA correlations leads to further quenching.

The RPWIA cross section results can give guidance when calculating the RDWIA LL' contributions because fitting calculations and final results for a specific combination in the RDWIA can be compared immediately to the RPWIA result to check for consistent behavior. RPWIA results also show that the LL' combinations can be arranged according to the relative magnitude of their contributions to the cross section. By calculating the LL' contributions with the largest effect on the cross section first, one can obtain a clearer picture of the final RDWIA result fairly early on.

V. CONCLUSION

We have shown how a standard RIA treatment of scattering and the assumption of a two-body SPVAT form for the nuclear current operator can be used to formulate a fully relativistic model for inclusive quasielastic nucleon-nucleus scattering. An important feature of our model is the separation of projectile and target responses into separate and independent tensors. This allows for the combination of different models for the projectile and the target. We performed a baseline calculation by modeling the projectile and ejectile as relativistic plane waves (RPWIA) and using a relativistic nuclear-matter description for the target (MFT). It was shown how the target description could be extended to include particle-hole correlations (RPA). In addition, we presented the formalism for incorporating distortion effects on the projectile and ejectile (RDWIA) as well as techniques for optimizing this highly nontrivial calculation.

Preliminary results for the polarized double differential cross section look promising. The familiar quasielastic peak is obtained. The peak widens and moves to higher energy transfer with a decrease in the effective mass of nucleons in the target. In addition, it moves to higher energy transfer and decreases with an increase in the scattering angle. Isoscalar RPA correlations tend to soften and reduce the nuclear response and therefore the magnitude of the quasielastic peak

owing to the attractive particle-hole interaction. This effect increases with increasing target density. It is also expected to increase with a lowering in beam energy owing to an increase in the apparent density of the target. At lower scattering angles this effect is slightly enhanced. Finally, the modulation of the projectile and ejectile wave functions by the nuclear potential (RDWIA) decreases the cross section when compared to the RPWIA result.

Nevertheless, some work remains to be done to obtain a more complete picture of the effects of the RPA and RDWIA.

The effect of the RPA on the double differential cross section could be enhanced if isovector (ρ and π) correlations are also taken into consideration. In fact, if the model is to be applied to quasielastic $(\vec{p},\vec{n})$ reactions, the isovector correlations become very important because these reactions probe only the isovector response of the nucleus. Our attempt here was simply to demonstrate the application of the RPA to our model of proton-nucleus scattering. The form of Eq. (80), however, allows for a straightforward inclusion of isovector RPA correlations similar to that of Ref. [2]. This would entail the construction of an additional medium-modified interaction for the isovector channel by specifying the free-space interaction matrix of the π and ρ mesons as well as the mixed polarization matrix as determined by the coupling of the isovector mesons to the nucleon.

Judging by Figs. 4 and 5 the amount of partial waves currently used is not yet satisfactory. Furthermore, all LL' contributions to the distorted wave cross section need to be calculated to obtain information on the spin-orbit distortion in addition to the quenching effect observed here. Unfortunately, the extreme numerical effort makes both of these undertakings very time consuming. Nonetheless, guided by the plane-wave results in determining the relative importance of different LL' contributions, progress on this front is a certainty.

Finally, one would like to calculate spin observables but using the formalism presented here it is a straightforward calculation as shown in Appendix D.

ACKNOWLEDGMENTS

B.I.S.v.d.V. wishes to acknowledge the financial support of the National Research Foundation (NRF) of South Africa under Grant No. GUN2048567. D.D.v.N. gratefully acknowledges financial support from the NRF, the Institute of Theoretical Physics at Stellenbosch University as well as the Fulbright Program. D.D.v.N. thanks the Physics Department, the Nuclear Theory Center and Prof. C. J. Horowitz at Indiana University for the hospitality extended to him during his stay in Bloomington, where part of this work was carried out. The authors also wish to thank Prof. J. Piekarewicz (Florida State University, USA) for helpful comments and suggestions.

APPENDIX A: DERIVATION OF THE EJECTILE DISTORTED WAVE FUNCTION

The Dirac wave function with incoming boundary conditions used for the ejectile is defined in terms of the time-reversal operator given by [38,65]

$$\mathcal{T} = TK, \tag{A1}$$

where K is the complex conjugation operator and

$$T = i\gamma^1\gamma^3 = \begin{bmatrix} -\sigma_2 & 0 \\ 0 & -\sigma_2 \end{bmatrix}. \tag{A2}$$

An energy projection operator $\Lambda_\rho(\mathbf{k}, M)$ (where $\rho = \pm$), is given by

$$\Lambda_\rho(\mathbf{k}, M) = \sum_s U^{(\rho)}(\mathbf{p}, s)\,\bar{U}^{(\rho)}(\mathbf{p}, s) = \left(\frac{\rho\ \not{k} + M}{2M}\right), \tag{A3}$$

where $U^{(+)}(\mathbf{p}, s) = U(\mathbf{p}, s)$ and $U^{(-)}(\mathbf{p}, s) = V(\mathbf{p}, s)$ refer to positive and negative energy solutions of the free Dirac equation. Using the identities

$$U(\mathbf{k}, \hat{i}', s') = \left(\frac{2M}{E(\mathbf{k}) + M}\right)^{\frac{1}{2}} \Lambda_+(\mathbf{k}, M)\, U(\mathbf{0}, \hat{i}', s'), \tag{A4}$$

$$\mathcal{T}\,\Lambda_+(\mathbf{k}, M)\,\mathcal{T}^{-1} = \Lambda_+(-\mathbf{k}, M), \tag{A5}$$

and

$$\mathcal{T}\,U(\mathbf{0}, \hat{i}', s') = i(-1)^{\frac{1}{2}+s'} U(\mathbf{0}, \hat{i}', -s'), \tag{A6}$$

it follows that

$$\mathcal{T}[\psi^{(+)}(\mathbf{x}, \mathbf{k}, \hat{i}, s)] = i(-1)^{\frac{1}{2}+s}\psi^{(+)}(\mathbf{x}, -\mathbf{k}, \hat{i}, -s). \tag{A7}$$

To obtain the wave function with incoming boundary conditions with the correct sign for the momentum and spin we therefore define it as

$$\psi^{(-)}(\mathbf{x}, \mathbf{k}, \hat{i}, s) = -i(-1)^{s-\frac{1}{2}}\mathcal{T}[\psi^{(+)}(\mathbf{x}, -\mathbf{k}, \hat{i}, -s)]. \tag{A8}$$

Because we cannot fix the direction of the ejectile momentum as we did for the projectile, Eq. (37) must be used when evaluating Eq. (A8) for the distorted wave with outgoing boundary conditions:

$$\begin{aligned}\psi^{(-)}(\mathbf{x}, \mathbf{k}, \hat{i}, s) &= -i(-1)^{s-\frac{1}{2}} TK[\psi^{(+)}(\mathbf{x}, -\mathbf{k}, \hat{i}, -s)] \\ &= -i(-1)^{s-\frac{1}{2}} i\gamma^1\gamma^3[\psi^{(+)}(\mathbf{x}, -\mathbf{k}, \hat{i}, -s)]^* \\ &= -i(-1)^{s-\frac{1}{2}} \begin{bmatrix} -\sigma_2 & 0 \\ 0 & -\sigma_2 \end{bmatrix} \\ &\quad \times [\psi^{(+)}(\mathbf{x}, -\mathbf{k}, \hat{i}, -s)]^*,\end{aligned} \tag{A9}$$

where

$$\begin{aligned}&[\psi^{(+)}(\mathbf{x}, -\mathbf{k}, \hat{i}, -s)]^* \\ &= \frac{4\pi}{kx}\left(\frac{E(\mathbf{k}) + M}{2M}\right)^{\frac{1}{2}} \sum_{ljms_z} (i^l)^* e^{-i\delta_{lj}} \\ &\quad \times \left\langle l\,\frac{1}{2}\, m s_z \middle| j, m + s_z \right\rangle \left[\mathcal{D}^{(\frac{1}{2})}_{s_z,-s}(\hat{i})\right]^* Y_{lm}(-\hat{k}) \\ &\quad \times \begin{bmatrix} g^*_{lj}(kx)\mathcal{Y}^*_{lj,m+s_z}(\hat{x}) \\ -if^*_{2j-l,j}(kx)\mathcal{Y}^*_{2j-l,j,m+s_z}(\hat{x}) \end{bmatrix}.\end{aligned} \tag{A10}$$

Using the identities

$$(i^l)^* = (-i)^l = (-1)^l i^l, \tag{A11}$$

$$\left[\mathcal{D}^{(\frac{1}{2})}_{s_z,-s}(\hat{i})\right]^* = (-1)^{s_z-(-s)}\mathcal{D}^{(\frac{1}{2})}_{-s_z,s}(\hat{i}) = (-1)^{s_z+s}\mathcal{D}^{(\frac{1}{2})}_{-s_z,s}(\hat{i}), \tag{A12}$$

$$Y_{lm}(-\hat{k}) = (-1)^l Y_{lm}(\hat{k}), \tag{A13}$$

we write Eq. (A10) as

$$\begin{aligned}[\psi^{(+)}(\mathbf{x},-\mathbf{k},\hat{i},-s)]^* &= \frac{4\pi}{kx}\left(\frac{E(\mathbf{k})+M}{2M}\right)^{\frac{1}{2}}\sum_{ljms_z}(-1)^{2l}i^l(-1)^{s_z+s}e^{-i\delta_{lj}} \\ &\times\left\langle l\tfrac{1}{2}ms_z\middle| j,m+s_z\right\rangle\mathcal{D}^{(\frac{1}{2})}_{-s_z,s}(\hat{i})Y_{lm}(\hat{k}) \\ &\times\begin{bmatrix} g^*_{lj}(kx)\mathcal{Y}^*_{lj,m+s_z}(\hat{x}) \\ -if^*_{2j-l,j}(kx)\mathcal{Y}^*_{2j-l,j,m+s_z}(\hat{x})\end{bmatrix}.\end{aligned} \tag{A14}$$

Use of this expression in Eq. (A9) as well as the fact that $(-1)^{2l} = 1$ (because $l \in \mathcal{Z}$) yields

$$\begin{aligned}\psi^{(-)}(\mathbf{x},\mathbf{k},\hat{i},s) &= -i(-1)^{s-\frac{1}{2}}\frac{4\pi}{kx}\left(\frac{E(\mathbf{k})+M}{2M}\right)^{\frac{1}{2}}\sum_{ljms_z}i^l(-1)^{s_z+s}e^{-i\delta_{lj}} \\ &\times\left\langle l\tfrac{1}{2}ms_z\middle| j,m+s_z\right\rangle\mathcal{D}^{(\frac{1}{2})}_{-s_z,s}(\hat{i})Y_{lm}(\hat{k}) \\ &\times\begin{bmatrix} g^*_{lj}(kx)(-\sigma_2\mathcal{Y}^*_{lj,m+s_z}(\hat{x})) \\ -if^*_{2j-l,j}(kx)(-\sigma_2\mathcal{Y}^*_{2j-l,j,m+s_z}(\hat{x}))\end{bmatrix}.\end{aligned} \tag{A15}$$

We now investigate the effect of the Pauli matrix σ_2 on the spin-spherical harmonics $\mathcal{Y}_{ljm}$. From the definition of the spin-spherical harmonic as

$$\mathcal{Y}_{lj\mu}(\hat{x}) = \sum_{t'_z}\left\langle l\tfrac{1}{2},\mu-t'_z,t'_z\middle| j\mu\right\rangle Y_{l,\mu-t'_z}(\hat{x})\chi_{t'_z}, \tag{A16}$$

it follows that

$$\mathcal{Y}^*_{lj\mu}(\hat{x}) = \sum_{t'_z}\left\langle l\tfrac{1}{2},\mu-t'_z,t'_z\middle| j\mu\right\rangle Y^*_{l,\mu-t'_z}(\hat{x})\chi_{t'_z}. \tag{A17}$$

Using the fact that $Y^*_{lm}(\hat{x}) = (-1)^m Y_{l,-m}(\hat{x})$, we can write

$$-\sigma_2\mathcal{Y}^*_{lj\mu}(\hat{x}) = \sum_{s'_z}\left\langle l\tfrac{1}{2},\mu-s'_z,s'_z\middle| j\mu\right\rangle(-1)^{\mu-s'_z}Y_{l,s'_z-\mu}(\hat{x})\left(-\sigma_2\chi_{s'_z}\right). \tag{A18}$$

The effect of the Pauli matrix on the spinor is

$$-\sigma_2\chi_{s'_z} = i(-1)^{s'_z+\frac{1}{2}}\chi_{-s'_z}, \tag{A19}$$

which leaves Eq. (A18) in the form

$$-\sigma_2\mathcal{Y}^*_{lj\mu}(\hat{x}) = i(-1)^{\mu+\frac{1}{2}}\sum_{t'_z}\left\langle l\tfrac{1}{2},\mu+t'_z,-t'_z\middle| j\mu\right\rangle Y_{l,\mu+t'_z}(\hat{x})\chi_{t'_z}, \tag{A20}$$

where we have relabeled the summation index $-s'_z \to t'_z$. If we rewrite Eq. (A16) as

$$\mathcal{Y}_{lj,-\mu}(\hat{x}) = \sum_{t'_z}\left\langle l\tfrac{1}{2},-(\mu+t'_z),t'_z\middle| j,-\mu\right\rangle Y_{l,\mu+t'_z}(\hat{x})\chi_{t'_z}, \tag{A21}$$

it bears a striking resemblance to Eq. (A20). The similarity becomes even more apparent if we make use of the following identity for the Clebsch-Gordon coefficients:

$$\langle j_1 j_2 m_1 m_2|jm\rangle = (-1)^{j_1+j_2-j}\langle j_1 j_2,-m_1,-m_2|j,-m\rangle, \tag{A22}$$

which implies that

$$\left\langle l\tfrac{1}{2},\mu+t'_z,-t'_z\middle| j\mu\right\rangle = (-1)^{l+\frac{1}{2}-j}\left\langle l\tfrac{1}{2},-(\mu+t'_z),t_z\middle| j,-\mu\right\rangle. \tag{A23}$$

Therefore, Eq. (A20) can be written as

$$-\sigma_2\mathcal{Y}^*_{lj\mu}(\hat{x}) = i(-1)^{l+\mu-j+1}\mathcal{Y}_{lj,-\mu}(\hat{x}). \tag{A24}$$

Recasting the expression into a form appropriate for Eq. (A15) yields

$$\begin{aligned}\psi^{(-)}(\mathbf{x},\mathbf{k},\hat{i},s) &= -i(-1)^{s-\frac{1}{2}}\frac{4\pi}{kx}\left(\frac{E(\mathbf{k})+M}{2M}\right)^{\frac{1}{2}}\sum_{ljms_z}i^l(-1)^{s_z+s}e^{-i\delta_{lj}} \\ &\times\left\langle l\tfrac{1}{2}ms_z\middle| j,m+s_z\right\rangle\mathcal{D}^{(\frac{1}{2})}_{-s_z,s}(\hat{i})\,Y_{lm}(\hat{k}) \\ &\times\begin{bmatrix} g^*_{lj}(kx)\,i(-1)^{l+m+s_z-j+1}\mathcal{Y}_{lj,-(m+s_z)}(\hat{x}) \\ -if^*_{2j-l,j}(kx)\,i(-1)^{m+s_z+j-l+1}\mathcal{Y}_{2j-l,j,-(m+s_z)}(\hat{x})\end{bmatrix}.\end{aligned} \tag{A25}$$

APPENDIX B: POLARIZATION TENSORS

A. Imaginary parts of the polarization tensors

Expressions for the imaginary parts of the polarization tensors for $LL' = SS$, VV, and AA agree with those derived in Refs. [21] and [24]. The expression for $LL' = TT$ has to our knowledge never been published for $\lambda^T = \sigma^{\mu\nu}$ owing to the form-factor parametrization ($\lambda^T = i\sigma^{\mu\nu}q_\mu/2M$) employed by most authors (see Refs. [24] and [27]). In addition, the expressions for $LL' = SV$ and VS agree with those derived in Refs. [21] and [24]. We have derived expressions for the imaginary parts of all LL' combinations as shown in Ref. [37].

The imaginary parts of the density-dependent polarization tensors are calculated according to Eq. (68). We choose $q^\mu = (q^0, 0, 0, |\mathbf{q}|)$ and define

$$E_n = \frac{E^n_{\text{upper}} - E^n_{\text{lower}}}{n}, \tag{B1}$$

where E_{upper} and E_{lower} are given by

$$E_{\text{upper}} = E_F, \tag{B2}$$

$$E_{\text{max}} = \max\left[M^*, E_{\text{upper}} - q^0, \frac{1}{2}\left(-q^0 + |\mathbf{q}|\sqrt{1 - \frac{4M^{*2}}{q_\mu^2}}\right)\right], \tag{B3}$$

$$E_{\text{lower}} = \min\left[E_{\text{max}}, E_{\text{upper}}\right]. \tag{B4}$$

We then obtain: $\text{Im}(\Pi^{SS}) = -\frac{(4M^{*2} - q_\mu^2)}{8\pi|\mathbf{q}|}E_1,$ (B5)

$\text{Im}(\Pi^{SV})$ and similarly for $\text{Im}(\Pi^{VS})$:

$$\text{Im}(\Pi^0) = -\frac{M^*}{4\pi|\mathbf{q}|}[2E_2 + q^0 E_1], \tag{B6}$$

$$\text{Im}(\Pi^3) = -\frac{M^* q^0}{4\pi|\mathbf{q}|^2}[2E_2 + q^0 E_1]. \tag{B7}$$

$\text{Im}(\Pi^{VV})$:

$$\text{Im}(\Pi^{00}) = -\frac{1}{2\pi|\mathbf{q}|}\left[E_3 + q^0 E_2 + \frac{q_\mu^2}{4}E_1\right], \tag{B8}$$

$$\text{Im}(\Pi^{03}) = \frac{q^0}{|\mathbf{q}|}\text{Im}(\Pi^{00}), \tag{B9}$$

$$\text{Im}(\Pi^{30}) = \text{Im}(\Pi^{03}), \tag{B10}$$

$$\text{Im}(\Pi^{33}) = \left[\frac{q^0}{|\mathbf{q}|}\right]^2 \text{Im}(\Pi^{00}), \tag{B11}$$

$$\text{Im}(\Pi^{11}) = \frac{q_\mu^2}{4\pi|\mathbf{q}|^3}\left[E_3 + q^0 E_2 + \left(\frac{|\mathbf{q}|^2 M^{*2}}{q_\mu^2} + \frac{q_0^2 + |\mathbf{q}|^2}{4}\right)E_1\right], \tag{B12}$$

$$\text{Im}(\Pi^{22}) = \text{Im}(\Pi^{11}). \tag{B13}$$

$\text{Im}(\Pi^{AA})$:

$$\text{Im}(\Pi^{AA}) = \text{Im}(\Pi^{VV}) + g^{\mu\nu}\left[\frac{M^{*2}E_1}{2\pi|\mathbf{q}|}\right]. \tag{B14}$$

$\text{Im}(\Pi^{TT})$: Five types of terms occur. Listed below are the expressions and the corresponding entries in the tensor:

$$\frac{-1}{4\pi|\mathbf{q}|^3}\left\{\left[q_0^2 + |\mathbf{q}|^2\right]\left[E_3 + q^0 E_2 + \frac{q_\mu^2}{4}E_1\right] - |\mathbf{q}|^2 M^{*2} E_1\right\}$$
$$= \text{Im}(\Pi^{0101}),\ -\text{Im}(\Pi^{0110}),\ \text{Im}(\Pi^{0202}),\ -\text{Im}(\Pi^{0220}),$$
$$-\text{Im}(\Pi^{1001}),\ \text{Im}(\Pi^{1010}),\ -\text{Im}(\Pi^{2002}),\ \text{Im}(\Pi^{2020}); \tag{B15}$$

$$\frac{q^0}{2\pi|\mathbf{q}|^2}\left[E_3 + q^0 E_2 + \frac{q_\mu^2}{4}E_1\right]$$
$$= \text{Im}(\Pi^{0113}),\ -\text{Im}(\Pi^{0131}),\ \text{Im}(\Pi^{0223}),\ -\text{Im}(\Pi^{0232}),$$
$$-\text{Im}(\Pi^{1013}),\ \text{Im}(\Pi^{1031}),\ \text{Im}(\Pi^{1301}),\ -\text{Im}(\Pi^{1310}),$$
$$-\text{Im}(\Pi^{2023}),\ \text{Im}(\Pi^{2032}),\ \text{Im}(\Pi^{2302}),\ -\text{Im}(\Pi^{2320}),$$
$$-\text{Im}(\Pi^{3101}),\ \text{Im}(\Pi^{3110}),\ -\text{Im}(\Pi^{3202}),\ \text{Im}(\Pi^{3220}); \tag{B16}$$

$$\frac{q_\mu^2}{2\pi|\mathbf{q}|^3}\left[E_3 + q_0 E_2 + \left(\frac{q_0^2}{4} + \frac{M^{*2}|\mathbf{q}|^2}{q_\mu^2}\right)E_1\right]$$
$$= \text{Im}(\Pi^{0303}),\ -\text{Im}(\Pi^{0330}),\ -\text{Im}(\Pi^{3003}),\ \text{Im}(\Pi^{3030}); \tag{B17}$$

$$\frac{q_\mu^2}{2\pi|\mathbf{q}|^3}\left\{E_3 + q_0 E_2 + \frac{q_0^2}{4}E_1 + \frac{q_0^3}{24}\right\}$$
$$= \text{Im}(\Pi^{1212}),\ -\text{Im}(\Pi^{1221}),\ -\text{Im}(\Pi^{2112}),\ \text{Im}(\Pi^{2121}); \tag{B18}$$

$$\frac{-1}{4\pi|\mathbf{q}|^3}\left\{\left[q_0^2 + |\mathbf{q}|^2\right]\left[E_3 + q^0 E_2 + \frac{q_\mu^2}{4}E_1\right] + |\mathbf{q}|^2 M^{*2} E_1\right\}$$
$$= \text{Im}(\Pi^{1313}),\ -\text{Im}(\Pi^{1331}),\ \text{Im}(\Pi^{2323}),\ -\text{Im}(\Pi^{2332}),$$
$$-\text{Im}(\Pi^{3113}),\ \text{Im}(\Pi^{3131}),\ -\text{Im}(\Pi^{3223}),\ \text{Im}(\Pi^{3232}). \tag{B19}$$

B. Real parts of the polarization tensors

Numerical results for the real parts of $LL' = SS,\ SV$, and VV are in exact agreement with the results obtained when using the analytical expressions published in Ref. [21]. Expressions for the real parts of other terms have, to our knowledge, not been published. We have derived expressions for the real parts of all LL' combinations as shown in Ref. [37]. The real parts of the density-dependent polarization tensors are calculated according to Eq. (67). The angular integrals are performed analytically and we list the results below. We choose $q^\mu = (q^0, 0, 0, |\mathbf{q}|)$ and define

$$L_1(k, q) = \log\left|2E_k^* q^0 - 2|\mathbf{k}||\mathbf{q}| - q_\mu^2\right|, \tag{B20}$$

$$L_2(k, q) = \log\left|2E_k^* q^0 + 2|\mathbf{k}||\mathbf{q}| - q_\mu^2\right|, \tag{B21}$$

$$L_3(k, q) = \log\left|2E_k^* q^0 - 2|\mathbf{k}||\mathbf{q}| + q_\mu^2\right|, \tag{B22}$$

$$L_4(k, q) = \log\left|2E_k^* q^0 + 2|\mathbf{k}||\mathbf{q}| + q_\mu^2\right|, \tag{B23}$$

$$L_{ij} = L_i - L_j, \tag{B24}$$

$$L_{ij\pm kl} = L_{ij} \pm L_{kl} \tag{B25}$$

and

$$E_L = (2E_k^* - q^0)L_{12} - (2E_k^* + q^0)L_{34}. \tag{B26}$$

We then obtain: $I_\theta^{SS} = \frac{(4M^{*2} - q_\mu^2)(L_{12-34}) + 8|\mathbf{k}||\mathbf{q}|}{|\mathbf{k}||\mathbf{q}|}.$ (B27)

I_θ^{SV} and similarly for I_θ^{VS}:

$$I_\theta^0 = \frac{2M^*}{|\mathbf{k}||\mathbf{q}|} E_L, \tag{B28}$$

$$I_\theta^3 = \frac{q^0}{|\mathbf{q}|} I_\theta^0. \tag{B29}$$

I_θ^{VV}:

$$I_\theta^{00} = \frac{1}{|\mathbf{k}||\mathbf{q}|}\left[\left(4E_k^{*2} + q_\mu^2\right) L_{12-34} - 4E_k q^0 L_{12+34} - 8|\mathbf{k}||\mathbf{q}|\right], \tag{B30}$$

$$I_\theta^{03} = \frac{q^0}{|\mathbf{q}|} I_\theta^{00}, \tag{B31}$$

$$I_\theta^{30} = I_\theta^{03}, \tag{B32}$$

$$I_\theta^{33} = \left[\frac{q^0}{|\mathbf{q}|}\right]^2 I_\theta^{00}, \tag{B33}$$

$$I_\theta^{11} = \frac{1}{2|\mathbf{k}||\mathbf{q}|^3}\left\{\left[4|\mathbf{k}|^2|\mathbf{q}|^2 - 4E_k^{*2} q_0^2 - q_\mu^2\left(q_0^2 + q^2\right)\right] L_{12-34} + 4E_k^* q^0 q_\mu^2 L_{12+34} + 8|\mathbf{k}||\mathbf{q}|\left(q_0^2 + q^2\right)\right\}, \tag{B34}$$

$$I_\theta^{22} = I_\theta^{11}. \tag{B35}$$

APPENDIX C: MEDIUM-MODIFIED PROPAGATOR

The medium-modified interaction is constructed according to Eq. (73) as a symbolic matrix product and inverted analytically resulting in a 5×5 matrix with nonzero components $\tilde{D}_{ij}$ $(i, j = -1, 0, 1, 2, 3)$ given by

$$\tilde{D}_{-1-1} = \frac{D^{(\sigma)}\left[\Pi^{00}\left(D_{00}^{(\omega)} - f^2 D_{00}^{(\omega)}\right) - 1\right]}{A}, \tag{C1}$$

$$\tilde{D}_{-10} = \tilde{D}_{0-1} = -\frac{\Pi^{S0} D^{(\sigma)} D_{00}^{(\omega)}}{A}, \tag{C2}$$

$$\tilde{D}_{-13} = \tilde{D}_{3-1} = \frac{f\Pi^{S0} D^{(\sigma)} D_{00}^{(\omega)}}{A}, \tag{C3}$$

$$\tilde{D}_{00} = \frac{D_{00}^{(\omega)}\{-[D^{(\sigma)}(\Pi^{S0})^2 + \Pi^{00} - \Pi^{00}\Pi^{SS} D^{(\sigma)}] D_{00}^{(\omega)} f^2 + \Pi^{SS} D^{(\sigma)} - 1\}}{A}, \tag{C4}$$

$$\tilde{D}_{03} = \tilde{D}_{30} = \frac{f[D^{(\sigma)}(\Pi^{S0})^2 + \Pi^{00} - \Pi^{00}\Pi^{SS} D^{(\sigma)}]\left(D_{00}^{(\omega)}\right)^2}{A}, \tag{C5}$$

$$\tilde{D}_{11} = \tilde{D}_{22} = -\frac{D_{00}^{(\omega)}}{\Pi^{22} D_{00}^{(\omega)} + 1}, \tag{C6}$$

$$\tilde{D}_{33} = \frac{D_{00}^{(\omega)}\left\{-[D^{(\sigma)}(\Pi^{S0})^2 + \Pi^{00}] D_{00}^{(\omega)} + \Pi^{SS} D^{(\sigma)}\left(\Pi^{00} D_{00}^{(\omega)} - 1\right) + 1\right\}}{A}, \tag{C7}$$

where

$$A = \Pi^{SS} D^{(\sigma)} - (f^2 - 1)[D^{(\sigma)}(\Pi^{S0})^2 + \Pi^{00} - \Pi^{00}\Pi^{SS} D^{(\sigma)}] D_{00}^{(\omega)} - 1, \tag{C8}$$

$$f = \frac{q^0}{|\mathbf{q}|}. \tag{C9}$$

APPENDIX D: SPIN OBSERVABLES

Note that in this formalism spin observables are defined as linear combinations of polarized double differential cross sections. For simplicity we let

$$d\sigma_{s_f s_i} = \frac{d\sigma}{d\Omega' dE'}(s_i, s_f), \tag{D1}$$

where $s_i = (j, s)$ and $s_f = (i', s')$ refer to the initial and final spin polarizations, respectively, and $j \in \{\hat{l}; \hat{s}; \hat{n}\}$ and $i' \in \{\hat{l}'; \hat{s}'; \hat{n}'\}$ as shown in Fig. 11.

We introduce the shorthand notation u_j to designate the spin projection $s = \frac{1}{2}$ (up) along direction j and d_j to designate the spin projection direction $s = -\frac{1}{2}$ (down) along direction j. Spin observables can then be calculated using [2,3,51,66]

$$D_{i'j} = \frac{d\sigma_{u_{i'}u_j} - d\sigma_{d_{i'}u_j} - d\sigma_{u_{i'}d_j} + d\sigma_{d_{i'}d_j}}{d\sigma_{u_{i'}u_j} + d\sigma_{d_{i'}u_j} + d\sigma_{u_{i'}d_j} + d\sigma_{d_{i'}d_j}}, \tag{D2}$$

where the denominator is clearly the unpolarized double differential cross section. The analyzing power A_y is the ratio of initially polarized nucleons left unpolarized after interacting with the target nucleus and can be calculated using

$$A_y = \frac{\left(d\sigma_{u_{i'}u_j} + d\sigma_{d_{i'}u_j}\right) - \left(d\sigma_{u_{i'}d_j} + d\sigma_{d_{i'}d_j}\right)}{d\sigma_{u_{i'}u_j} + d\sigma_{d_{i'}u_j} + d\sigma_{u_{i'}d_j} + d\sigma_{d_{i'}d_j}}. \tag{D3}$$

The polarization can be calculated using

$$P = \frac{\left(d\sigma_{u_{i'}u_j} + d\sigma_{u_{i'}d_j}\right) - \left(d\sigma_{d_{i'}u_j} + d\sigma_{d_{i'}d_j}\right)}{d\sigma_{u_{i'}u_j} + d\sigma_{d_{i'}u_j} + d\sigma_{u_{i'}d_j} + d\sigma_{d_{i'}d_j}}. \tag{D4}$$

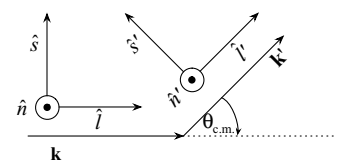

FIG. 11. Definition of the spin projection axes used for the calculation of spin observables in the center-of-mass frame.

[1] C. J. Horowitz and D. P. Murdock, Phys. Rev. C **37**, 2032 (1988).
[2] C. J. Horowitz and J. Piekarewicz, Phys. Rev. C **50**, 2540 (1994).
[3] G. C. Hillhouse, Ph.D. thesis, Stellenbosch University, 1999.
[4] C. J. Horowitz and M. J. Iqbal, Phys. Rev. C **33**, 2059 (1986).
[5] K. Wehrberger and F. Beck, Phys. Lett. B **270**, 1 (1991).
[6] R. D. Smith and S. J. Wallace, Phys. Rev. C **32**, 1654 (1985).
[7] T. A. Carey, K. W. Jones, J. B. McClelland, J. M. Moss, L. B. Rees, N. Tanaka, and A. D. Bacher, Phys. Rev. Lett. **53**, 144 (1984).
[8] T. Chen, R. E. Segel, P. T. Debevec, J. Wiggins, P. P. Singh, and J. V. Maher, Phys. Lett. B **103**, 192 (1981).
[9] J. S. Wesick, P. G. Roos, N. S. Chant, C. C. Chang, A. Nadasen, L. Rees, N. R. Yoder, A. A. Cowley, S. J. Mills, and W. W. Jacobs, Phys. Rev. C **32**, 1474 (1985).
[10] J. A. Tjon and S. J. Wallace, Phys. Rev. Lett. **54**, 1357 (1985).
[11] C. J. Horowitz and J. Piekarewicz, Phys. Lett. B **301**, 321 (1993).
[12] L. Ray and G. W. Hoffmann, Phys. Rev. C **31**, 538 (1985).
[13] L. Ray, G. W. Hoffmann, M. L. Barlett, J. J. Jarmer, B. C. Clark, R. E. Kozack, R. L. Mercer, G. R. Burleson, and S. Hama, Phys. Rev. Lett. **56**, 2465 (1986).
[14] O. Häusser *et al.*, Phys. Rev. Lett. **61**, 822 (1988).
[15] O. Häusser *et al.*, Phys. Rev. C **43**, 230 (1991).
[16] M. Ichimura, K. Kawahigashi, T. S. Jørgensen, and C. Gaarde, Phys. Rev. C **39**, 1446 (1989).
[17] K. Kawahigashi, K. Nishida, A. Itabashi, and M. Ichimura, Phys. Rev. C **63**, 044609 (2001).
[18] B. D. Serot and J. D. Walecka, in *Advances in Nuclear Physics* (Plenum, New York, 1986), Vol. 16.
[19] C. J. Horowitz and B. D. Serot, Nucl. Phys. A **368**, 503 (1981).
[20] J. F. Dawson and R. J. Furnstahl, Phys. Rev. C **42**, 2009 (1990).
[21] K. Wehrberger, Phys. Rep. **225**, 273 (1993).
[22] B. D. Serot and J. D. Walecka, Int. J. Mod. Phys. E **6**, 515 (1997).
[23] G. C. Hillhouse and P. R. De Kock, Phys. Rev. C **49**, 391 (1994).
[24] H. Kim, Ph.D. thesis, Indiana University, 1995.
[25] J. Piekarewicz, Phys. Rev. C **64**, 024307 (2001).
[26] C. J. Horowitz and J. Piekarewicz, Phys. Rev. C **47**, 2924 (1993).
[27] C. J. Horowitz and K. Wehrberger, Nucl. Phys. A **531**, 665 (1991).
[28] A. L. Fetter and J. D. Walecka, *Quantum Theory of Many-particle System* (McGraw-Hill, New York, 1971).
[29] J. Piekarewicz, Phys. Rev. C **62**, 051304 (2000).
[30] H. Kurasawa and T. Suzuki, Nucl. Phys. A **445**, 685 (1985).
[31] H. Kurasawa and T. Suzuki, Phys. Lett. B **173**, 377 (1986).
[32] K. Wehrberger and F. Beck, Phys. Rev. C **35**, 298 (1987).
[33] K. Wehrberger and F. Beck, Phys. Rev. C **37**, 1148 (1988).
[34] C. J. Horowitz and J. Piekarewicz, Phys. Rev. Lett. **62**, 391 (1989).
[35] C. J. Horowitz and J. Piekarewicz, Nucl. Phys. A **511**, 461 (1990).
[36] J. Piekarewicz and J. R. Shepard, Phys. Rev. C **51**, 806 (1995).
[37] D. D. Van Niekerk, Ph.D. thesis, Stellenbosch University, 2010.
[38] J. D. Bjorken and S. Drell, *Relativistic Quantum Mechanics* (McGraw-Hill, New York, 1964).
[39] J. A. McNeil, J. R. Shepard, and S. J. Wallace, Phys. Rev. Lett. **50**, 1439 (1983).
[40] J. A. McNeil, L. Ray, and S. J. Wallace, Phys. Rev. C **27**, 2123 (1983).
[41] D. P. Murdock and C. J. Horowitz, Phys. Rev. C **35**, 1442 (1987).
[42] G. C. Hillhouse, B. I. S. van der Ventel, S. M. Wyngaardt, and P. R. De Kock, Phys. Rev. C **57**, 448 (1998).
[43] J. R. Shepard, E. Rost, and J. Piekarewicz, Phys. Rev. C **30**, 1604 (1984).
[44] E. Rost and J. R. Shepard, Phys. Rev. C **35**, 681 (1987).
[45] C. J. Horowitz, Phys. Rev. C **31**, 1340 (1985).
[46] M. Ichimura and K. Kawahigashi, Phys. Rev. C **45**, 1822 (1992).
[47] J. A. Tjon and S. J. Wallace, Phys. Rev. C **32**, 1667 (1985).
[48] J. A. Tjon and S. J. Wallace, Phys. Rev. C **32**, 267 (1985).
[49] J. A. Tjon and S. J. Wallace, Phys. Rev. C **35**, 280 (1987).
[50] J. A. Tjon and S. J. Wallace, Phys. Rev. C **36**, 1085 (1987).
[51] B. I. S. Van der Ventel, Ph.D. thesis, Stellenbosch University, 1999.
[52] E. Rost, J. R. Shepard, E. R. Siciliano, and J. A. McNeil, Phys. Rev. C **29**, 209 (1984).
[53] D. Sebilleau, J. Phys. A **31**, 7157 (1998).
[54] S. A. Chin, Ann. Phys. **108**, 301 (1977).
[55] H. C. Jean, J. Piekarewicz, and A. G. Williams, Phys. Rev. C **49**, 1981 (1994).
[56] C. J. Horowitz, Nucl. Phys. A **412**, 228 (1984).
[57] K. Lim and C. J. Horowitz, Nucl. Phys. A **501**, 729 (1989).
[58] J. Rasch and A. C. H. Yu, SIAM J. Sci. Comput. **25**, 1416 (2003).
[59] D. Pinchon and P. E. Hoggan, Int. J. Quantum Chem. **107**, 2186 (2007).
[60] W. Press, S. A. Teukolsky, W. Vetterling, and B. P. Flannery, *Numerical Recipes in Fortran*, 2nd ed. (Cambridge University Press, New York, 1992).
[61] D. Levin, Math. Comput. **38**, 531 (1982).
[62] D. Levin, J. Comput. Appl. Math. **67**, 95 (1996).
[63] G. A. Evans and J. R. Webster, J. Comput. Appl. Math. **112**, 55 (1999).
[64] J. Li, X. Wang, T. Wang, and C. Shen, Appl. Math. Comput. **209**, 327 (2009).
[65] G. R. Satchler, *Direct Nuclear Reactions* (Oxord University Press, New York, 1983).
[66] B. I. S. van der Ventel, G. C. Hillhouse, and P. R. De Kock, Phys. Rev. C **62**, 024609 (2000).